João Nuno Vidal Félix

Licenciado em Ciências da Engenharia Eletrotécnica e de Computadores

Quasi-Optimum Detection of Nonlinear MIMO Signals

Dissertação para obtenção do Grau de Mestre em

Engenharia Electrotécnica e de Computadores

Orientador:	Rui Miguel Henriques Dias Morgado Dinis, Professor Associado com Agregação, Faculdade de Ciências e Tecnologia - Universidade Nova de Lisboa
Co-orientador:	João Francisco Martinho Lêdo Guerreiro, Professor Auxiliar, Universidade Autónoma de Lisboa

Júri

Presidente:	Doutor Luís Augusto Bica Gomes de Oliveira - FCT/UNL
Arguente:	Doutor Luís Filipe Lourenço Bernardo - FCT/UNL
Vogal:	Doutor João Francisco Martinho Lêdo Guerreiro - UAL

FACULDADE DE CIÊNCIAS E TECNOLOGIA
UNIVERSIDADE NOVA DE LISBOA

Setembro, 2019

Quasi-Optimum Detection of Nonlinear MIMO Signals

Este documento foi gerado utilizando o processador (pdf)LaTeX, com base no template "novathesis" [1] desenvolvido no Dep. Informática da FCT-NOVA [2].
[1] https://github.com/joaomlourenco/novathesis [2] http://www.di.fct.unl.pt

"Life is and will ever remain an equation incapable of solution, but it contains certain known factors"
Nicolas Tesla

Acknowledgements

Firstly, i would like to express that this dissertation would not be possible to be written if i could not count with all the support given by my adviser Prof. Dr. Rui Dinis, who help me through all the stages and during all these months. I also want to express my gratitude to Prof. Dr. João Guerreiro, for all the advices and for guiding me on the preparation of the scientific research.

I would like to appreciate to all my family. This whole growth process as a citizen and as a student is due to my parents, Isabel and José, and they know how grateful I am for that. This dissertation is dedicated to my grandparents, Julieta and Orlando, for all the love they gave me, for everything they taught me and for always helping me to chase my dreams. I know that they are very proud of me, although we can not celebrate together.

I would also like to give my special thanks to my girlfriend, Margarida, for all the love, support and patient that she had. Thanks for always believing me.

During all these six years i shall thanks all my friends to be with me in this chapter. For all the advices, friendship and encouragement.

Abstract

It is widely known that multiple-input, multiple-output (MIMO) transmission techniques lead to signals with substantial envelope fluctuations which increases the sensitivity of nonlinear distortion effects. The existence of nonlinear distortion in the transmitted signals can substantially prejudice the system performance, leading to high irreducible error floors. However, it has been recently demonstrated that the nonlinear distortion has useful information on the transmitted signals which means that, surprisingly, it can be used to improve the performance. However the distortion effects can only be exploited by the optimum receiver, which presents a very high complexity. In this work, sub-optimum receivers which less complexity are proposed. These sub-optimum receivers are based on the belief propagation (BP) and on the generalized approximate message passing (GAMP). It is shown that their performance can be substantially better than the performance of conventional receivers that considered the nonlinear distortion as noise. Moreover, for both MIMO orthogonal frequency division multiplexing (OFDM) and MIMO single-carrier with frequency-domain equalization (SC-FDE) systems, it is demonstrated that the performance in the presence of nonlinear distortion effects generated by low-resolution quantization processes can be even better than the performance assuming a linear, high-resolution quantization.

Keywords: MIMO, OFDM, SC-FDE, nonlinear distortion, message passing,GAMP, decoding

Resumo

É do conhecimento geral que as técnicas de transmissão com múltiplas entradas e saídas (MIMO) conduzem a sinais com grandes flutuações de envolvente, o que aumenta a sensibilidade aos efeitos da distorção não linear. A existência de distorções não lineares nos sinais transmitidos podem prejudicar substancialmente o desempenho do sistema, levando a níveis elevados de erros. No entanto, tem sido demonstrado recentemente que a distorção não linear tem informações úteis sobre os sinais transmitidos, o que significa que, surpreendentemente, ela pode ser usada para melhorar o desempenho. No entanto, os receptores óptimos podem apresentar uma elevada complexidade. Assim, neste trabalho o receptor implementado tem o intuito de reduzir a complexidade do sistema. Estes receptores sub-ótimos são baseados na propagação de mensagens (BP) e no algoritmo GAMP. Mostra-se que seu desempenho pode ser substancialmente melhor do que o desempenho de receptores convencionais que consideravam a distorção não linear como ruído. Além disso, tanto para os sistemas MIMO-OFDM quanto para MIMO SC-FDE, é demonstrado que o desempenho na presença de efeitos de distorção não linear gerados por processos de quantização de baixa resolução pode ser ainda melhor do que o desempenho assumindo quantização linear de alta resolução.

Palavras-chave: MIMO, OFDM, SC-FDE, Distorção não linear, message passing, GAMP, descodificação

Contents

List of Figures

Acronyms

ADC Analog-to-digital Converter

AMP Approximate Message Passing

AWGN Additive White Gaussian Noise

BER Bit Error Rate

BP Belief Propagation

CLT Central Limit Theorem

CP Cyclic Prefix

CSI Channel State Information

DAC Digital-to-analog Converter

DCT Discrete Cosine Transform

DFT Discrete Fourier Transform

FDE Frequency-domain Equalization

FDM Frequency Division Multiplexing

FFT Fast Fourier Transform

GAMP Generalized Approximate Message Passing

HPA High Power Amplifiers

IB-DFE Iterative Block - Decision Feedback Equalizer

ICI Inter-carrier Interference

IDFT Inverse Discrete Fourier Transform

IFFT Inverse Fast Fourier Transform

ISI Inter-symbol interference

LDPC Low Density Parity Check

LLR Log-likelihood Ratio

LoS Line of Sight

LTE Long Term Evolution

MAP *maximum a posteriori* probability

MCMC Markov Chain Monte Carlo

MIMO Multiple-input Multiple-output

ML Maximum Likelihood

MMSE Minimum Mean-squared Error

OFDM Orthogonal Frequency Division Multiplexing

PAPR Peak-to-average Power Ratio

PDF Probability Density Function

PSD Power Spectral Density

QAM Quadrature Amplitude Modulation

QPSK Quadrature Phase Shift Keying

RF Radio Frequency

SC-FDE Single Carrier Frequency Domain Equalization

SISO Single-Input Single-Output

SMC Sequential Monte Carlo

SNR Signal-noise Ratio

SQNR Signal-to-quantization Noise Ratio

SSPA Solid State Power Amplifier

SVD Singular Value Decomposition

TWTA Traveling Wave Tube Amplifier

ZF Zero-forcing

Symbols

$\boldsymbol{A}$ decoding SVD orthogonal matrix

a_i Tanner graph check nodes

A_i set of position of ones in ith row of parity check matrix

$A_{i/j}$ set of A_i except the bit of jth position

α scaling factor of the nonlinear component

A_s amplitude of output saturation

b number of quantization bits

$\boldsymbol{B}$ precoding SVD orthogonal matrix

β_m vector of adopted constellation scheme

b_j bit nodes of Tanner graph

B_j set of position of ones in jth column of parity check matrix

$B_{j/i}$ set of B_j except the bit of ith position

$\boldsymbol{\alpha}_k$ SC-FDE feedback equalization matrix

C number of parallel data streams

$(.)^*$ complex conjugate operation

$\boldsymbol{D}_k$ nonlinear distorted term at kth subcarrier

E_b energy per bit

$E_{j/i}$ extrinsic message from check node j to bit node i

$E[(.)]$ expectation of (.)

$f_A(.)$ AM/AM conversion characteristic

$\boldsymbol{F}_k^{(i)}$ SC-FDE feedforward equalization matrix at kth subcarrier and ith iteration

$\boldsymbol{F}_k$ coefficients of OFDM channel equalization at kth subcarrier

$f_P(.)$ AM/PM conversion characteristic

$\boldsymbol{G}$ LDPC generator matrix

g_{in} input GAMP function

g_{out} output GAMP function

$\boldsymbol{H}$ matrix of channel impulsive response

$h_{(N_R,N_T)}$ channel matrix coefficients at N_R and N_T antennas

$(.)^H$ hermitian matrix operation

$\boldsymbol{H}_k$ channel impulsive response at kth subcarrier

$\mathbf{I}$ identity matrix

J oversampling factor

Λ diagonal matrix of singular value decomposition

$\lambda_k^{(c)}$ singular values matrix for cth stream and kth subcarrier

L_i *a priori* probability message

M number of constellation points

$M_{j/i}$ intrinsic message arrived at check nodes

N signal block size

N_0 power spectral density of the channel noise

n_{it} number of GAMP iteration

$\boldsymbol{N}_k$ frequency-domain AWGN factor at kth subcarrier

N_R number of reception antennas

$\mathbf{n}^{'}$ decoded SVD noise signal

N_T number of transmission antennas

$\boldsymbol{\nu}_n$ AWGN samples

$\mathbf{n}$ noise vector

p smoothness factor

$p(x_j)$ *a priori* probability at jth input node

ρ correlation factor

$\mathbf{S}_k$ frequency-domain transmitted OFDM signal at kth subcarrier

$\mathbf{s}_n$ time-domain transmitted OFDM signal at nth sample

$\tilde{\boldsymbol{S}}_k$ frequency-domain OFDM estimated signal

syn syndrome

$\boldsymbol{\theta}$ LDPC parity check matrix

T_s symbol duration time

$(.)^T$ transpose matrix operation

$\mu^{(.)}$ variance of (.) GAMP component

σ_n noise variance

$var[(.)]$ variance of (.)

σ_x OFDM signal variance

$\mathbf{x}(n_{it})$ decoded GAMP vector

$\hat{\mathbf{x}}^{\mathbf{SP}}$ decoded vector of sum-product algorithm

$\hat{x}_j$ estimated GAMP input component for each j input node

$\boldsymbol{X}_k$ frequency-domain precoded signal at kth subcarrier

$\mathbf{x}_n$ modulated GAMP data symbols

x_n time-domain sample

$\mathbf{x}^{'}$ precoded SVD signal

$\mathbf{x}$ transmitted vector

y_i GAMP output component for each i output node

$\boldsymbol{Y}_k$ frequency-domain received signal for each k subcarrier

$\mathbf{y}_n$ received GAMP data symbols

$\mathbf{y}^{'}$ decoded SVD signal

$\mathbf{y}$ received vector

$\boldsymbol{Z}_k$ nonlinear distorted signal at kth subcarrier

$\mathbf{z}_n$ nonlinear GAMP transformation vector

$\boldsymbol{z}_n$ nonlinearity output data symbols

Chapter 1

Introduction

1.1 Context and Motivation

Over the years, it has been observed a dilatation of offered services for the majority of communication systems. Therefore, it has been possible to provide new services and applications, such as, 4K video transmission, internet of things, among others. The OFDM is a frequency division multiplexing (FDM) technique. However, the spectrum of each subcarrier can overlap which leads to an increased spectral efficiency. This work considers an OFDM technique together with a cyclic prefix (CP) for simple, low-complex frequency-domain equalization (FDE). The OFDM is one of the most spectral efficient technique and it can, in the same way, transmit data with high bit rate in severely time-dispersive channels. The evolution of the equipment used in this transmission technique was substantially felt when it was applied the Discrete Cosine Transform (DCT) on baseband circuits. Thereafter, it has emerged the Fast Fourier Transform (FFT), and, as a consequence, the number of arithmetic operations decreased from N^2 to $Nlog(N)$ [LaS+08]. However, there are some factors that can affect the performance of OFDM systems, leading to an increase of bit error rate (BER). In fact, the OFDM technique is characterized by high envelope fluctuation, which guide to an high peak-to-average power ratio (PAPR). Large PAPR leads to amplification difficulties, which normally results in a decreased battery lifetime of the transmitter.

Other important aspect of OFDM transmission systems is the receiver synchronization. According to the literature, synchronization issues can compromise the subcarriers orthogonality, which, consequently, decreases the signal-noise ratio

(SNR) and cause inter-symbol interference (ISI) and inter-carrier interference (ICI) [San+98].

Despite these disadvantages, OFDM offers a great flexibility and resilience to multi-path fading. Therefore, it has been selected for several standards, for instance, IEEE 802.11 and 5G [Afa+16; Rap+13]. Thus, the study of OFDM schemes was one of the main point of this dissertation, more concretely, the performance analysis of OFDM systems with nonlinear distortion effects.

On the other hand, it is used single carrier transmission techniques with frequency-domain equalization, so-called SC-FDE, which is an alternative to OFDM. These two transmission techniques can be integrated on the mobile wireless system, while the OFDM handles with downlink and the SC-FDE handles with uplink transmission. This allows a given wireless mobile communication system to maintain the complexity on base station and reduce the complexity on mobile terminals, not to mention the increase in the power efficiency.

MIMO techniques have been present in mostly wireless communication to achieve better system capacity [AFS10]. However, when submitted to a nonlinear device, MIMO signals can face strong distortion levels, although MIMO schemes can have robustness to nonlinear distortion at the transmitter side when the number of transmit antennas is much higher than the number of independent data streams [Gue+16a; Gue+16b]. In fact, the performance degradation due to nonlinear distortion effects for conventional receivers can be substantial, with large irreducible error rates, especially for the modes associated to the weakest singular values [Gue+16a].

Nevertheless, for single-input, single-output (SISO) systems it has been shown that when Maximum Likelihood (ML) receivers are employed, the nonlinear distortion effects can be used to improve the performance, instead of being considered prejudicial [Gue+15]. The goal of this thesis is to study nonlinear MIMO systems, both OFDM and SC-FDE, and to verify if the optimum detection can be an alternative to the conventional detection. Due to the large complexity of optimum receivers, sub-optimal receivers based on the GAMP concept are proposed.

1.2 Organization

This dissertation has two principal aims: (1) to implement a receiver to deal with distortion term introduced by the high power amplifiers (HPA) and Analog-to-Digital Converters (ADC) or Digital-to-analog Converters (DAC), based on GAMP algorithm and (2) to apply the implemented receiver to a MIMO system, which is able to deal with the problems of the nonlinear distortion. It is also organized in four principal chapters. In Chap. 2, firstly it is analyzed a MIMO channel scheme as well as its singular value decomposition (SVD). After that, it is characterized the MIMO OFDM and SC-FDE transmission technique. It is also described the nonlinear distortion effects introduced on the transmission process. Concerning Chap. 3, it is made an overview about low density parity-check (LDPC) codes and the decoding algorithms based on BP, in order to extend the receiver design. In Chap. 4 it is presented the implemented GAMP receiver design for the previous described systems, as well as performance results. Last, Chap. 5 concludes the dissertation briefly describing all considered important points of the developed work and a future implementations.

1.3 Contributions

The main contribution of this thesis was the development of practical, sub-optimum receivers for MIMO systems that can take advantage of nonlinear distortion effects to improve the performance. This contribution has lead to two conference papers, namely:

- J. Felix, J. Guerreiro, and R.Dinis. "On the detection of MIMO signals with strong nonlinear distortion effects." in: IEEE Vehicular Technology Society (VTC)-Fall, Hawaii, USA, September 2019,
- J. Felix, J. Guerreiro, R. Dinis and P.Montezuma . "Reduced-Complexity Quasi-Optimum Detection for MIMO-OFDM Signals with Strong Nonlinear Distortion." To be presented at IEEE Global Communications Conference (GLOBECOM) Workshops, Hawaii, USA, December 2019.

Chapter 2

State-of-Art

On a communication system, it is called MIMO scheme when it is used more than one antenna at the transmitter and receiver side. Over the years MIMO has been gained popularity on Long Term Evolution (LTE) and has been assumed as a system with N_T transmission antennas and N_R reception antennas, which allows spatial diversity. This scheme is adopted for wireless communication in order to achieve better spectral efficiency and better system performance on a narrow bandwidth, as well as to accomplish the next generation of wireless networks.

Thus, it is possible to state that signals between receivers and transmitters antennas are present in the spectrum of frequencies due to the propagation phenomenon. As a consequence of what was been written, radio stations can communicate with mobile terminals through the multi-path propagations. Considering a Single-input Single-output (SISO) system, it is important to note that the same block of data can be received through wireless communication, in different time instants, by means of reflection, refraction and diffraction in objects. Certainly, these effects will cause interference on received signal, namely ISI. On the other hand, it is possible that the received signal frequency differs from the frequency of the transmitted signal (i.e., Doppler shift), which is another undesired effect of the propagation channel. These impairments can lead to performance degradation of wireless communication systems. Consequently, the design of communication system involves a trade-off between used power, bandwidth, bit rate, decoding quality and complexity of the receiver.

In particular, this chapter will refer to MIMO techniques such as MIMO OFDM and MIMO SC-FDE. In section 2.1, it is presented an overview of MIMO systems characterization and it is briefly described the fading channel. In section 2.2, it is presented the OFDM technology followed by MIMO OFDM system overview. Section 2.3 is dedicated to MIMO SC-FDE technique.

2.1 MIMO Communication Schemes

Let us start by considering a MIMO system represented by N_T antennas at transmitter and N_R antennas at receiver. It can be expressed by $N_T \times N_R$ configuration, which denotes the size of channel matrix, defined by $\mathbf{H}$. According to the MIMO configuration, we can have different architectures, i.e., $N_T > N_R$, $N_T < N_R$ or $N_T = N_R$. If the number of transmit antennas is greater or smaller than the number of receivers antennas, it is an unbalanced MIMO. Otherwise, it is a balanced. MIMO configuration, as is illustrated in Fig. 2.1.1.

In addiction, as illustrated in Fig. 2.1.1, each receive antenna receives signals from all transmission antennas. If each antenna is too close to the next one, it may cause correlation between them, which might reduce the diversity gains of the MIMO system. The channel matrix $\mathbf{H}$ with dimension $N_T \times N_R$ is given by

$$\mathbf{H} = \begin{bmatrix} h_{(1,1)} & h_{(1,2)} & \cdots & h_{(1,n_T)} \\ h_{(2,1)} & h_{(2,2)} & \cdots & h_{(2,n_T)} \\ \vdots & \vdots & \ddots & \vdots \\ h_{(n_R,1)} & h_{(n_R,2)} & \cdots & h_{(N_R,N_T)} \end{bmatrix}, \tag{2.1}$$

where each coefficient of matrix $\mathbf{H}$ determines the relationship between each $n_T : (1,2,\cdots,N_T)$ transmission antenna and $n_R : (1,2,\cdots,N_R)$ reception antenna (i.e., it is the channel response between a given pair of antennas).

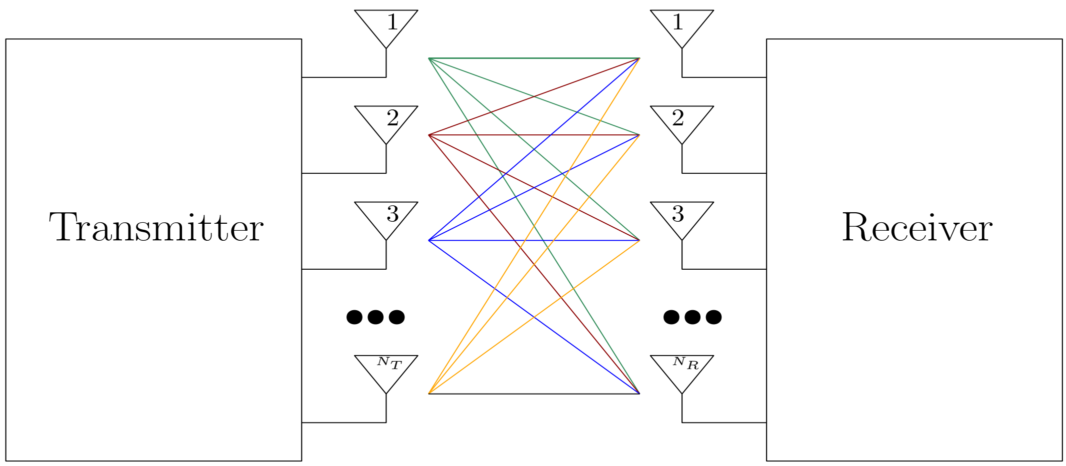

Figure 2.1.1: MIMO transmission scheme for a $N_T \times N_R$ antenna configuration.

If the delay spread is small, the coherence bandwidth will be greater than signal bandwidth. Consequently, the channel matrix remains constant across all the frequency and it can be defined as a flat fading channel over the available bandwidth. Otherwise, if the delay spread is large and the coherence bandwidth is smaller than signal bandwidth the channel is considered frequency-selective.

Let us consider that the signal transmitted by the N_T antennas is represented as $\mathbf{x} = [x^{(1)}, x^{(2)}, \cdots, x^{(N_T)}]$ and is transmitted over a MIMO channel. Nevertheless, signals are perturbed by noise $\mathbf{n} \in \mathbb{C}^{N_R \times 1}$, such as additive white Gaussian noise (AWGN), which results on $\mathbf{y} \in \mathbb{C}^{N_R \times 1}$ received signal, represented as a relationship between transmitted signal and channel plus noise perturbation.

In this work, the channel fading coefficients are modeled by a *Rayleigh* distribution, since their real and imaginary parts follow a Gaussian disruption with zero mean and unitary variance. Thus, the received signal can be expressed as

$$\mathbf{y} = \mathbf{H}\mathbf{x} + \mathbf{n}. \tag{2.2}$$

2.1.1 Singular Value Decomposition

In this subsection, the SVD decomposition is presented [Liu+09]. This transformation increases the complexity of the system, although some methods were proposed in order to reduce it [Wan+10]. In order to decouple the transmitted data streams, the SVD technique allows to decompose the channel matrix $\mathbf{H}$, presented in (2.1), in two orthogonal matrices, $\mathbf{A}$ and $\mathbf{B}$, and one diagonal matrix, Λ. This decomposition allows the parallel transmission of $C = min(N_T, N_R)$ streams. For this purpose, the MIMO channel matrix can be decomposed as

$$\mathbf{H} = \mathbf{A}\boldsymbol{\Lambda}\mathbf{B}^H, \tag{2.3}$$

where $\mathbf{A} \in \mathbb{C}^{N_R \times C}$ and $\mathbf{B} \in \mathbb{C}^{C \times N_T}$ are unitary matrices(i.e., $\mathbf{A}\mathbf{A}^{\mathbf{H}} = \mathbf{A}^{\mathbf{H}}\mathbf{A} = \mathbf{I}$). The Hermitian operation, i.e., the complex conjugate of the transpose of a matrix, is represented by $(.)^H$. The diagonal of matrix $\boldsymbol{\Lambda}$ has dimension $C \times C$ and it is also composed by non-zero singular values, $\lambda_1 \geqslant \lambda_2 \geqslant \cdots \geqslant \lambda_C$. In fact, the singular values of $\mathbf{H}$ are the eigenvalues of $\mathbf{H}\mathbf{H}^H$ and $\mathbf{H}^H\mathbf{H}$. The matrix description of a channel decomposition with $N_T = N_R$ is illustrated in Fig. 2.1.2.

By replacing (2.3) in (2.2), the received signal can be expressed as

$$\mathbf{y} = \mathbf{A}\boldsymbol{\Lambda}\mathbf{B}^H\mathbf{x} + \mathbf{n}. \tag{2.4}$$

In doing so, if it was applied a precoding operation, the precoded signal is presented as

$$\mathbf{x}^{'} = \mathbf{B}^{\mathbf{H}}\mathbf{x}.(2.5)$$

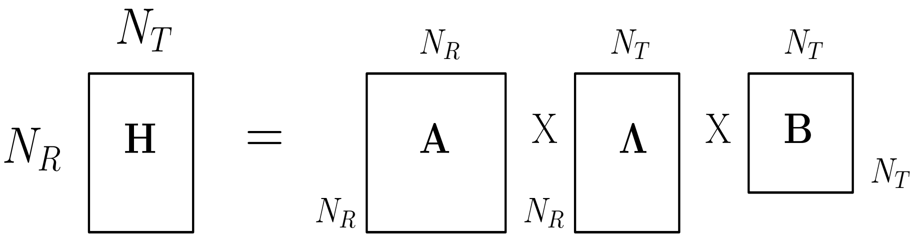

Figure 2.1.2: Matrix representation of SVD.

Consequently, in order to complete the reception with SVD, the decoded signal can be written as

$$\mathbf{y}^{'} = \mathbf{A}^{\mathbf{H}}\mathbf{y}, (2.6)$$

$$\mathbf{n}^{'} = \mathbf{A}^{\mathbf{H}}\mathbf{n}. (2.7)$$

Under this conditions, the received signal shown in (2.4), it could be written as

$$\mathbf{y}' = \mathbf{\Lambda}\mathbf{x}^{'} + \mathbf{n}^{'}. (2.8)$$

2.2 MIMO-OFDM

As is widely known OFDM technique is a multi-carrier modulation, which is based on a block transmission and normally combined with a CP. In the frequency-domain, the OFDM spectrum is a um of shifted *sinc* functions, where each *sinc* is associated to a given sub-channel. The orthogonality is maintained while sub-carriers are spaced by $1/T_s$. As a consequence, when a subcarrier has a maximum amplitude, in frequency-domain, the others are zero, which enables the over-lapping between sub-channels without interference. The signal is the sum of N independent signals, modulated in sub-channels with the same bandwidth. The use of a CP allows to increase the multi-path robustness and permits a simple FDE.

The OFDM is one of the most spectral efficient technique. It is showed by practical results in [Sam+02] that MIMO technique can lead to better performance and capacity than SISO systems. MIMO-OFDM techniques can be also contemplated as frequency-domain technique with frequency diversity, since the OFDM converts the selective frequency channel into a set of parallel flat-fading channels.

From the Central Limit Theorem (CLT) [PP02; Rud14], the time-domain OFDM signals have an approximate Gaussian distribution when the number of subcarriers N or the number of parallel data streams C is large. For this reason, the absolute value of the complex envelope can be approximate a Rayleigh distribution with zero-mean and variance $2\sigma_s^2$ (i.e., the real and imaginary parts of the signals are approximately Gaussian distributed with variance σ_s^2). In Fig. 2.2.1, it is showed the simulated and theoretical Probability Density Function (PDF) of the real part of a generated discrete-time OFDM signal, (i.e., $\mathfrak{Re}(x_n)$), in presence of $N = 64$ subcarriers. As can be observed, the Gaussian approximation is very tight.

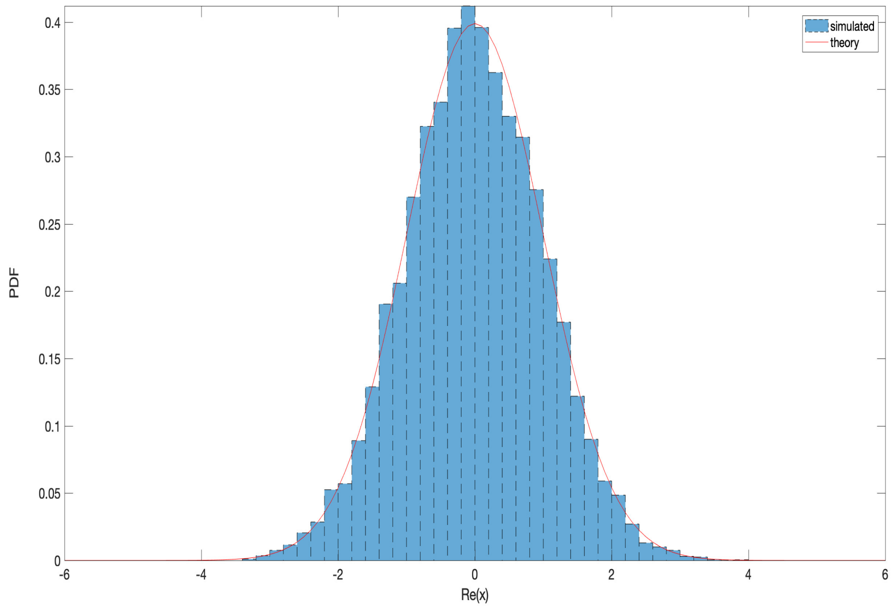

Figure 2.2.1: Simulated and theoretical PDF of the real part of a given OFDM signal.

Therefore, the complex envelope of the input signal can be regarded as a Rayleigh distribution [Hel+11]. Fig. 2.2.2 confirmed the previous sentence with the histogram of complex envelope of the OFDM symbol. Thus, the PDF of OFDM signal complex envelope is, approximately,

$$p(x) = \frac{1}{\sqrt{2\sigma_x^2\pi}} \exp\left(-\frac{x^2}{2\sigma_x^2}\right). \tag{2.9}$$

In modern wireless communications schemes, OFDM is combined with MIMO techniques to increase the system's capacity, although MIMO systems can be joined with other types of modulation or multiple-access techniques. As a side note, when it is applied the OFDM technique, each subcarrier can be seen as *flat-fading* channel as it was previously mentioned.

The OFDM signals are generated digitally through an Inverse Discrete Fourier Transform (IDFT) of a set of complex data symbols (for instance quadrature phase

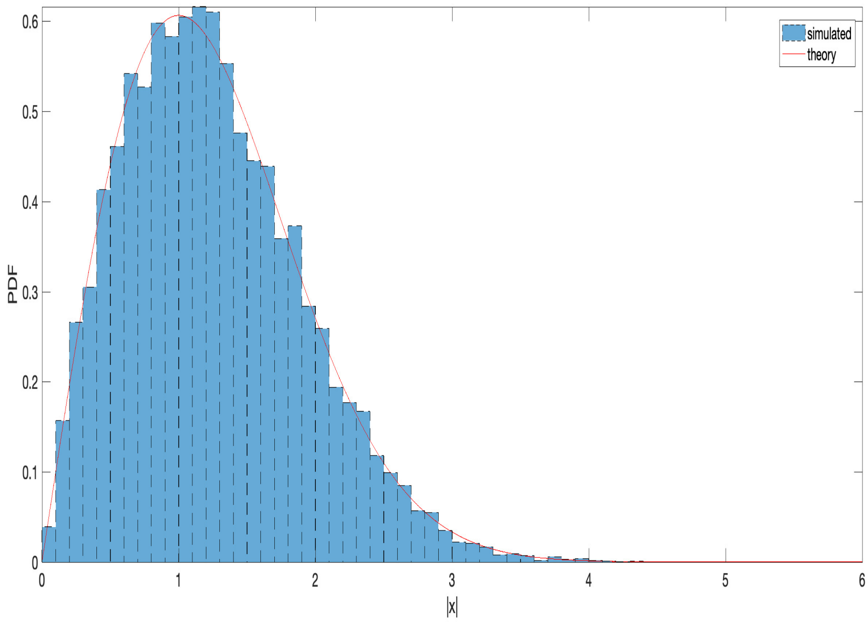

Figure 2.2.2: Simulated and theoretical PDF of complex envelope of OFDM signal.

shift keying (QPSK) symbols) $\mathbf{S}_k = [S_k^{(1)}, S_k^{(2)}, \cdots, S_k^{(C)}]^T$, which yields the time-domain samples $\mathbf{s}_n$, whereby the time domain block for the cth data stream is $\mathbf{s}_n^{(c)} = [s_0^{(1)}, s_1^{(2)}, ..., s_{N-1}^{(C)}]$. Usually, the OFDM symbols have an oversampling factor J (i.e., $(J-1)N$ null subcarriers are added to the N data subcarriers of each data block) to prevent aliasing effects. Thus, to the original block, on frequency-domain, $[\mathbf{S}_k; k = 0, 1, \cdots, N-1]$ zeros were added, half in the beginning and the other half in the end, which produces $[\mathbf{S}_k; k = \frac{-(J-1)N}{2}, \frac{-(J-1)N}{2} + 1, \cdots, \frac{(J-1)N}{2}]$.

Concerning to multi-carrier transmission, it is necessary to take into consideration the sensitivity to the nonlinear distortion effects, which can lead to both in-band distortion and out-of-band radiation.

Thanks to the Bussgang's theorem [Bus52], a nonlinearly distorted Gaussian signal can be decomposed as the sum of two uncorrelated components, one representing a scaled replica of the original signal and another representing the nonlinear distortion [Gus+05; Hel+11; Min85; Rap91; Row82]. Therefore, a nonlinearly distorted MIMO-OFDM signal can be represented as

$$\mathbf{Z}_k = \alpha \mathbf{S}_k + \mathbf{D}_k, \tag{2.10}$$

where α is a scale factor and $\mathbf{D}_k = [D_k^{(1)}, D_k^{(2)}, ..., D_k^{(N_T)}]^T$ represents the nonlinear distortion terms associated to the kth subcarrier. Under these conditions, the received signal is given by

$$\mathbf{Y}_k = \mathbf{H}_k \mathbf{Z}_k + \mathbf{N}_k, \tag{2.11}$$

where $\mathbf{N}_k = [N_k^{(1)}, N_k^{(2)}, ..., N_k^{(R)}]^T$ represents the set of AWGN samples associated to the kth subcarrier. These samples are modeled by a complex Gaussian distribution with $N_k \sim \mathcal{CN}(0, 2\sigma_N^2)$, where $\sigma_N^2 = N_0/2$ is the noise Power Spectral Density (PSD).

The channel matrix associated to a given subcarrier is defined as

$$\mathbf{H}_k = \begin{bmatrix} H_k^{(1,1)} & H_k^{(1,2)} & \cdots & H_k^{(1,T)} \\ H_k^{(2,1)} & H_k^{(2,2)} & \cdots & H_k^{(2,T)} \\ \vdots & \vdots & \ddots & \vdots \\ H_k^{(R,1)} & H_k^{(R,2)} & \cdots & H_k^{(R,T)}, \end{bmatrix}. \tag{2.12}$$

where $H_k^{(r,t)}$ represents the channel frequency response associated to the tth transmit antenna and rth receive antenna, for each kth subcarrier. The singular values of channel matrix can be related with channel equivalent gain $\lambda_k^{(c)} = [\lambda_k^{(1)}, \lambda_k^{(2)}, \cdots, \lambda_k^{(c)}]$, for cth stream and kth subcarrier. High order streams have worst system performance, producing high irreducible error floors [Gue+16a], [Gue+17].

By replacing (2.10) in (2.11), the received signal can be expressed by

$$\begin{aligned} \mathbf{Y}_k &= \mathbf{H}_k \mathbf{Z}_k + \mathbf{N}_k = \mathbf{H}_k(\alpha \mathbf{X}_k + \mathbf{D}_k) + \mathbf{N}_k \\ &= \alpha \mathbf{H}_k \mathbf{S}_k + \mathbf{H}_k \mathbf{D}_k + \mathbf{N}_k. \end{aligned}$$

The signal for detection purpose is obtained by the process of the signal equalization, leading to

$$\tilde{\mathbf{S}}_k = \mathbf{F}_k \mathbf{Y}_k, \tag{2.13}$$

where, $\mathbf{F}_k$ is the set of coefficients that compensates the channel effects, known as equalization matrix. The equalization can be enhanced under Zero-forcing (ZF) or Minimum Mean Square Error (MMSE) criterion. It is also performed on frequency-domain, where it is less complex than on time-domain.

The last task of the receiver is to convert the estimated data symbol, represented in (2.13), into a sequence of binary values. This process is performed regarding the modulation scheme used to generate the transmitted data symbol.

2.2.1 Sensitivity to Nonlinearity

In a real system, a radio frequency (RF) transmitter introduces non-linear distortions. In order to transmit data it is necessary to include High Power Amplifiers (HPA) at transmitter side, and the HPAs usually present a nonlinear characteristic. As far as it has been observed, there are possibilities to wield this problem, such as making the amplifier working in linear region with PAPR reduction schemes or applying Bussgang receivers and, as a consequence, estimating and cancelling the non-linear distortion term. However, when the PAPR of the signal is large, the nonlinear distortion effects are almost unavoidable [RM13].

2.2.1.1 High Power Amplifiers

There are many models to define non-linear amplification, for instance the Solid State Power Amplifier (SSPA) and the Traveling Wave Tube Amplifier (TWTA) model, which were studied and analyzed in [Hel+11; Rap91; Sal81]. These models involve an AM/AM distortion component and an AM/PM distortion component.

For an amplifier to be power efficient, it has to introduce a non-linear response to the system. There are some models to define the non-linearity of HPA, which are based on input/output observations with two specific characteristics, for instance, the AM/AM, amplitude distortion, and AM/PM, phase distortion.

Therefore, the input/output characteristic function of HPA block is represented by the complex envelope

$$f(z_n) = f_A(|x_n|)exp^{(jarg(x_n)+jf_P(|x_n|))}, \tag{2.14}$$

where f_A is the AM/AM conversion, and f_P is the AM/PM conversion.

The bandpass memoryless non-linearity can be represented by the non-linear block of Fig. 2.2.3.

Figure 2.2.3: Block diagram of bandpass memoryless non-linearity.

From the point of view developed in [Sal81], A.M Saleh defined a model in which was used the AM/AM and the AM/PM conversion functions, known as TWTA . They can be represented by

$$f_A(|x_n|) = \frac{a_0 \, |x_n|}{1 + a_1 \, |x_n|^2}, \tag{2.15}$$

and

$$f_P(|x_n|) = \frac{b_0 \, |x_n|}{1 + b_1 \, |x_n|^2}, \tag{2.16}$$

where a_0, a_1, b_0 and b_1 are the method coefficients. In the other hand, the AM/AM conversion can be defined on characteristic function, modeled by Rapp, in the so-called SSPA

$$f_A(|x_n|) = \frac{|x_n|}{[1 + (\frac{|x_n|}{A_s})^{2p}]^{\frac{1}{2p}}}, \tag{2.17}$$

where A_s represents the output saturation amplitude of the amplifier and the p is the smoothness factor of transition between linear and saturation region.

As a result of the low values of AM/PM conversion of SSPA, the Rapp model considers a null AM/PM characteristic [Rap91].

In this thesis, the severity of the nonlinearity is controlled by the normalized clipping level s_M/σ.

Fig. 2.2.4 shows the simulated BER of an OFDM system with $N = 512$ subcarriers, considering a nonlinear power amplifier parametrized with different values of s_M/σ. Clearly, the lower the s_M/σ, the stronger the distortion , which means that many signals samples will be in the non-linear region, leading to a worse performance. Fig. 2.2.5 shows the AM/AM characteristic of different nonlineari-

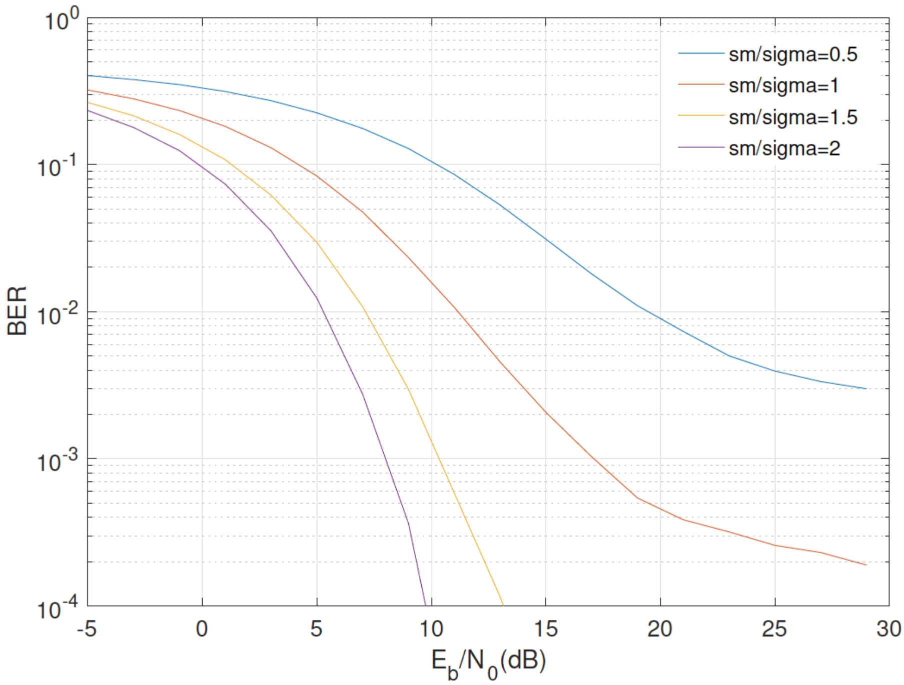

Figure 2.2.4: Simulated BER of an OFDM system impaired by a nonlinear PA considering different values of normalized clipping level.

ties. The transition from linear region to non-linear region can be well marked as the coordinate point (s_M, s_M). From the figure, it can be noted that when higher

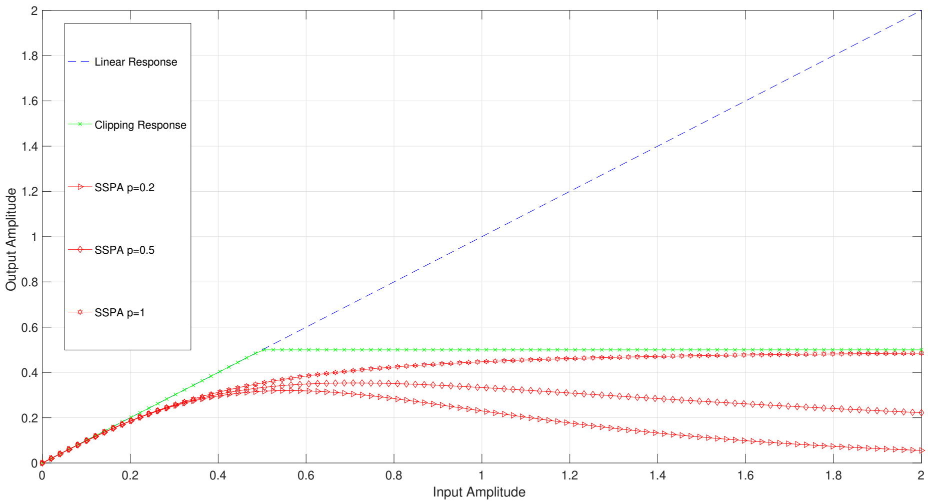

Figure 2.2.5: AM/AM characteristic of different nonlinearities, considering $s_M = 0.5$.

values of p are considered, the AM/AM characteristic of SSPA's approaches an ideal envelope clipping.

2.2.1.2 ADC and DAC

It is a requirement to employ analog-to-digital converters at both transmitter and receiver transmission chain, ADC and DAC, respectively, in order to send information through OFDM technique. The power consumption of these devices are proportional to the number of bits of resolution. The ADC's output at the nth time instant for the input x_n is

$$z_n = f\left(\mathfrak{Re}\left(x_n\right)\right) + jf\left(\mathfrak{Im}\left(x_n\right)\right), \tag{2.18}$$

where $f(\cdot)$ function represents a uniform quantization characteristic with b bits of resolution and normalized clipping level s_M/σ. The nonlinearity represented in (2.18) is known as an I-Q since it detaches the real part of the signal from the imaginary part, and each one produces the quantized value trough the function $f(\cdot) = fI(\cdot) = fQ(\cdot)$. For this purpose, in [Rib+15] is demonstrated that for a given number of bits of resolution, there is an optimum value of the normalized clipping level that minimizes the signal-to-quantization noise ratio (SQNR). In Fig. 2.2.6 it is illustrated the block diagram of I-Q nonlinearity.

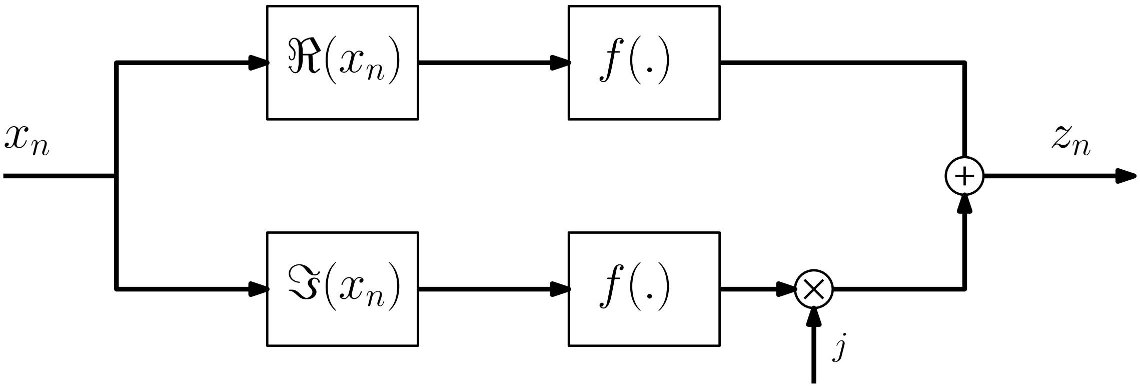

Figure 2.2.6: Block diagram of an I-Q nonlinearity.

2.2.2 Precoding and Preprocessing

The precoding and preprocessing operations are based on matrices $\mathbf{B}_k^H$ and $\mathbf{A}_k^H$, respectively. However, the precoding process requires the perfect knowledge of channel information at the transmitter and receiver side. Fig. 2.2.7 shows the considered transmitter structure and also represents the precoding operation at the transmitter based on the matrices $\mathbf{B}_k^H$. The separation of the different data streams is completed by the detection operation performed at the receiver side that is based on the matrices $\mathbf{A}_k^H$. It equally shows the positions of IDFT and DFT on transmitter and receiver side, respectively.

The precoding is done for each kth subcarrier by multiplying $\mathbf{S}_k$ with the precoding matrix $\mathbf{B}_k^H$, represented as

$$\mathbf{X}_k = \mathbf{B}_k^H \mathbf{S}_k. \tag{2.19}$$

Then, by substituting (2.19) in (2.20), the received signal can be expressed as

$$\begin{aligned}\mathbf{Y}_k &= \alpha \mathbf{A}_k \mathbf{\Lambda}_k \mathbf{B}_k \mathbf{B}^H \mathbf{S}_k + \mathbf{A}_k \mathbf{\Lambda}_k \mathbf{B}_k^H \mathbf{D}_k + \mathbf{N}_k \\ &= \alpha \mathbf{A}_k \mathbf{\Lambda}_k \mathbf{S}_k + \mathbf{A}_k \mathbf{\Lambda}_k \mathbf{B}_k \mathbf{D}_k + \mathbf{N}_k.\end{aligned} \tag{2.20}$$

The signal for detection purposes is obtained through the multiplication of the received signal with the decoding matrix $\mathbf{A}^H$, leading to

$$\tilde{\mathbf{S}}_k = \mathbf{A}_k^H \mathbf{Y}_k. \tag{2.21}$$

By combining (2.20) and (2.21), it is defined

$$\begin{aligned}\tilde{\mathbf{S}}_k &= \alpha \mathbf{A}_k^H \mathbf{A}_k \mathbf{\Lambda}_k \mathbf{S}_k + \mathbf{A}_k^H \mathbf{A}_k \mathbf{\Lambda}_k \mathbf{B}_k \mathbf{D}_k + \mathbf{A}_k^H \mathbf{N}_k. \\ &= \alpha \mathbf{\Lambda}_k \mathbf{S}_k + \mathbf{\Lambda}_k \underbrace{\mathbf{B}_k \mathbf{D}_k}_{\mathbf{D}'_k} + \mathbf{A}_k^H \mathbf{N}_k,\end{aligned} \tag{2.22}$$

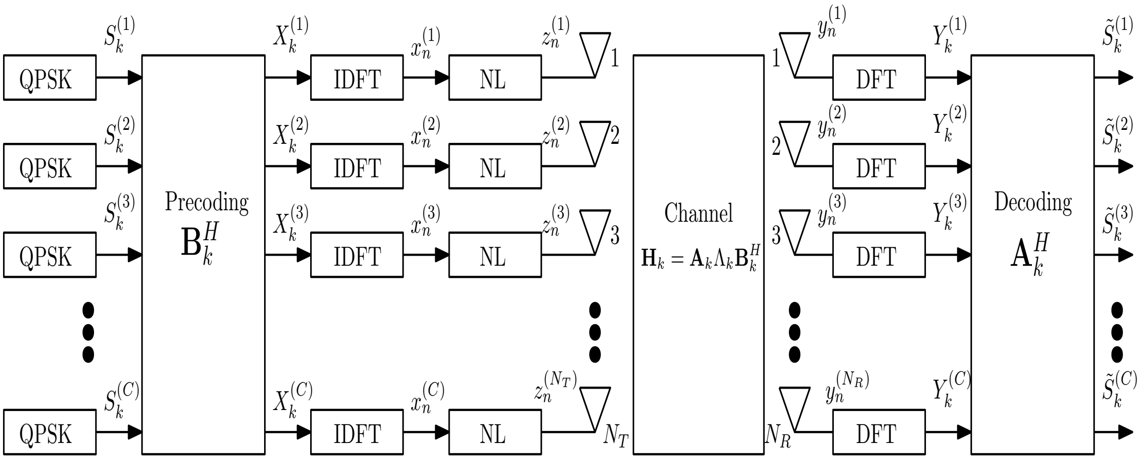

Figure 2.2.7: Basic MIMO-OFDM $N_T \times N_R$ scheme employing a SVD technique.

where $\mathbf{D}'_k$ is the nonlinear distortion term weighted by the precoding matrix.

To summarize, the precoding done at the transmitter is made through the matrix $\mathbf{B}_k^H$ and the separation of different data streams is done at the receiver by the preprocessing matrix $\mathbf{A}_k^H$.

2.3 MIMO-SC-FDE

Since OFDM signals present large envelope fluctuations and a high sensitivity to nonlinear distortion effects, single-carrier signals can be an alternative. In that context, the SC-FDE has been considered as an option for broadband wireless communications.

The difference between a MIMO-OFDM system and a MIMO-SC-FDE is the placement of the IFFT and FFT blocks. Therefore, the complexity of both techniques is comparable. Likewise, both transmission techniques can be combined with a CP to facilitate the equalization and reduce the ISI.

After the transmission process, the received block is passed to frequency-domain using DFT, where $(\mathbf{Y}_k : k = 0, 1, \cdots, N-1) = \mathrm{DFT}(\mathbf{y}_n; n = 0, 1, \cdots, N-1)$. Thus, the received signal can be described as

$$\mathbf{Y}_k = \mathbf{H}_k\mathbf{Z}_k + \mathbf{N}_k, \tag{2.23}$$

where $\mathbf{N}_k = [N_k^{(1)}, N_k^{(2)}, \cdots, N_k^{(R)}]^T$ is the set of frequency-domain AWGN samples, associated to each subcarrier.

The decoding operation of the receiver is employed by $\mathbf{A}^H$ for each subcarrier. Therefore, the decoded signal is given as

$$\tilde{\mathbf{S}}_k = \mathbf{A}_k^H\mathbf{Y}_k. \tag{2.24}$$

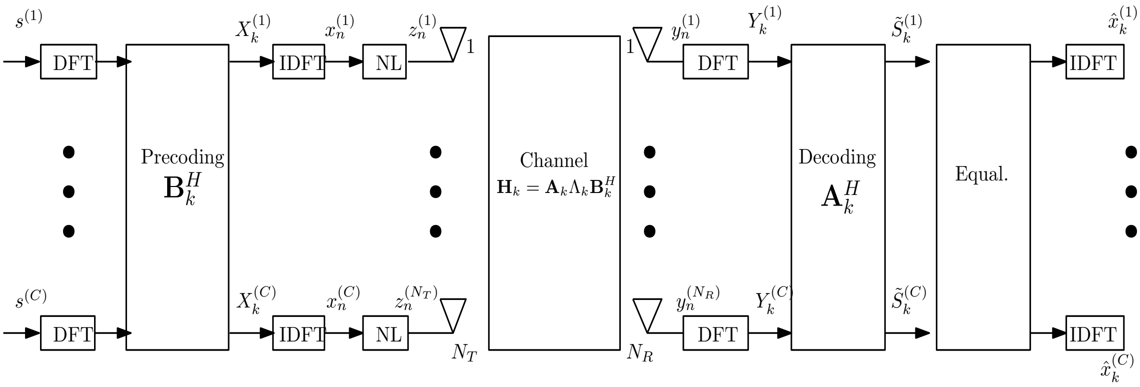

Figure 2.3.1: Basic MIMO SC-FDE $N_T \times N_R$ scheme employing a SVD technique.

By considering equation (2.23) and (2.24), it is obtained

$$
\begin{aligned}
\tilde{\mathbf{S}_k} &= \mathbf{A}_k^H \mathbf{H}_k \mathbf{Z}_k + \mathbf{A}_k^H \mathbf{N}_k \\
&= \mathbf{A}_k^H \mathbf{H}_k \mathbf{B}_k \mathbf{S}_k + \mathbf{A}_k^H \mathbf{N}_k \\
&= \mathbf{A}_k^H \mathbf{A}_k \boldsymbol{\Lambda}_k \mathbf{B}_k^H \mathbf{B}_k \mathbf{S}_k + \mathbf{A}_k^H \mathbf{N}_k \\
&= \alpha \boldsymbol{\Lambda}_k \mathbf{S}_k + \boldsymbol{\Lambda}_k \underbrace{\mathbf{B}^H \mathbf{D}_k}_{\mathbf{D}'_k} + \mathbf{A}_k^H \mathbf{N}_k,
\end{aligned}
\tag{2.25}
$$

where $\mathbf{D}'_k$ represents the nonlinear distortion term for detection purpose.

As it was shown in [Mad+19], the ordered singular values will impact differently on system performance, which is a consequence of frequency-selective channels. It can be assumed an Iterative Block Decision Feedback Equalizer (IB-DFE), which uses feed-forward and feedback equalization. As an iterative equalization, it has i number of iterations. For the first iteration, all coefficients are zero, which implies a linear FDE. The feed-forward and feedback equalization matrices can be expressed for each subcarrier k and iteration i, respectively, as

$$
\mathbf{F}_k^{(i)} = \frac{\boldsymbol{\Lambda}_k}{\left(1 - \left|\rho^{(i-1)}\right|^2\right) \boldsymbol{\Lambda}_k^2 + \frac{1}{SNR}},
\tag{2.26}
$$

where $\rho^{(i-1)}$ is the correlation factor and it is used the channel's SNR, and

$$
\boldsymbol{\alpha}_k^{(i)} = \mathbf{F}_k^{(i)} \boldsymbol{\Lambda}_k - \mathbf{I}_{N_R},
\tag{2.27}
$$

where I_{N_R} represents an identity matrix of size N_R.

The data set of equalized symbols for each subcarrier and iteration is represented by,

$$
\hat{\mathbf{S}}_k^{(i)} = \mathbf{F}_k^{(i)} \mathbf{Y}_k - \boldsymbol{\alpha}_k^{(i)} \hat{\mathbf{S}}_k^{(i-1)}.
\tag{2.28}
$$

For conventional receivers, a hard-decision can be considered to estimate the set of transmitted data, which implies $\hat{\mathbf{s}}_n = (Re(\tilde{\mathbf{x}}_n)) + j(Im(\tilde{\mathbf{x}}_n))$, after the final IDFT receiver operation. The block $\hat{\mathbf{S}}_k^{(i-1)}$ of previous equation is the DFT of block $\hat{\mathbf{s}}_n^{(i)}$, which denotes the hard-decision of previous FDE iteration.

Chapter 3

Generalized Approximate Message Passing

In any transmission technique, the receiver has the role of reconstructing the message that was sent to the transmitter. This can be difficult, because the received signal can be trough many impairments, for instance, channel disturbances and distortion effects introduced by the HPA. As a result, the received signal is susceptible to an arbitrary probability of error.

In Shannon's work [Sha48], the concept of information entropy was established, which represents the amount of lost information in the transmission, also seen as an uncertainty measure. It was also introduced the important concept of channel capacity, which is related to the mutual information in a communication system.

The scientific community has discussed the estimation of received signal in areas such as signal processing, image processing and machine-learning. The solution is based on probabilistic system methods, required to know how many random variables are present as well as to understand how they connect with each others.

Thomas Bayes was one of the probabilistic inference pioneer. He created a theorem about probabilistic inference, whereby he defined the conditional probability between random variables, which is used to know how probabilistic events behave. In [ÁT16] and [Wan+00], the authors reported methods and algorithms of Bayesian analyses, such as Markov Chain Monte Carlo (MCMC) and Sequential Monte Carlo (SMC). However, some of Bayesian methods can be computationally complex.

It follows that it is fundamental to express the need of implementing non-complex receivers to try to face the non-linearity problems. One of the decoding methods of LDPC codes is the Sum-Product Message Passing, also known as BP, which uses Tanner Graphs and Bayesian inference [Sho04]. Some investigations were realized to estimate the received values. Those signals were object of linear transformation and suffered an interference of AWGN in a reception data block, based on BP. In subsection 3.1.1, it is presented an overview of ?? codes. Subsection 3.1.2 is dedicated to the Sum-product.

One of the first algorithms was the Approximate Message Passing (AMP), suggest by [Don+09]. Later, the GAMP algorithm was proposed [Ran10]. Contrary to AMP, the GAMP can cope with nonlinear transformations. Recently, the GAMP concept was used as the basis of sub-optimum receivers for nonlinear OFDM, showing a great potential [Zhi17a; Zhi17b]. In [Zhi17b], it is shown that the information contained in the nonlinear distortion can be used to improve the performance.

The sub-optimum receiver uses the GAMP algorithm for QPSK constellations and considers AWGN channels. It is shown that the performance of the GAMP sub-optimum receiver can be even better than the performance of linear OFDM. In [Zhi17a], it is claimed the impact that the choice of non-linearity function can have in the system efficiency. The GAMP methods can also be used on compressive sensing [SR15].

3.1 Message Passing - Belief Propagation

3.1.1 LDPC codes

In 1962, when LDPC codes were proposed in [Gal63], it was far from its potential, since it required rigorous computational methods and do not compete against linear block codes and convolutional codes.

From the standpoint of linear block codes, it is turned possible to construct a message $\underline{b}$ with a certain number of bits, on a codeword $\underline{a}$ based on a generator matrix $\mathbf{G}$, i.e.,

$$\underline{b} = \underline{a}\mathbf{G}. \tag{3.1}$$

Thereby, the dimension of a code is represented by the number of bits of $\underline{a}$ times the number of bits $\underline{b}$. From the matrix $\mathbf{G}$, it is realizable to express the parity-check matrix $\boldsymbol{\theta}$. Additionally, it can be defined the weight of ones in the rows and the weigh of ones in the columns of $\boldsymbol{\theta}$, as w_r and w_c, respectively. This is a sparse matrix with low density of ones. For that matter, all matrices of this subsection have binary values.

Other important characteristic is the minimum distance between two codewords, d_{min}. Consequently, d_{min} results from the minimum number of columns of $\boldsymbol{\theta}$ which sums are zero.

In order to interpret sparse matrices, a *tanner graph* or *factor graph* was created to represent graphically the parity-check matrix. *Tanner graphs* are made by two type of nodes: (1) a check nodes, which are represented by the parity-check equations from each row of $\boldsymbol{\theta}$ and (2) b bit nodes, that are represented by the number of columns of $\boldsymbol{\theta}$. The connection between nodes matches with the number of ones in parity-check matrix. This information is based on the weight of ones on the rows and columns of $\boldsymbol{\theta}$. Fig. 3.1.1 represents a *tanner graph* of the matrix $\boldsymbol{\theta}$. As it can be seen, A_i denotes the set of positions of ones in the ith row of $\boldsymbol{\theta}$ and B_j the set of positions of ones in the jth column of $\boldsymbol{\theta}$, for instance $A_i = (2,4,5,8),(1,2,3,6),(3,6,7,8),(1,4,5,7)$ and $B_j = (2,4),(1,2),(2,3),(1,4),(2,3),(3,4),(1,3)$, respectively.

In order to decode LDPC codes, the exchange of messages between the tanner graph nodes can be used iteratively with beliefs about the nodes.

$$\boldsymbol{\theta} = \begin{bmatrix} 0 & 1 & 0 & 1 & 1 & 0 & 0 & 1 \\ 1 & 1 & 1 & 0 & 0 & 1 & 0 & 0 \\ 0 & 0 & 1 & 0 & 0 & 1 & 1 & 1 \\ 1 & 0 & 0 & 1 & 1 & 0 & 1 & 0 \end{bmatrix}$$

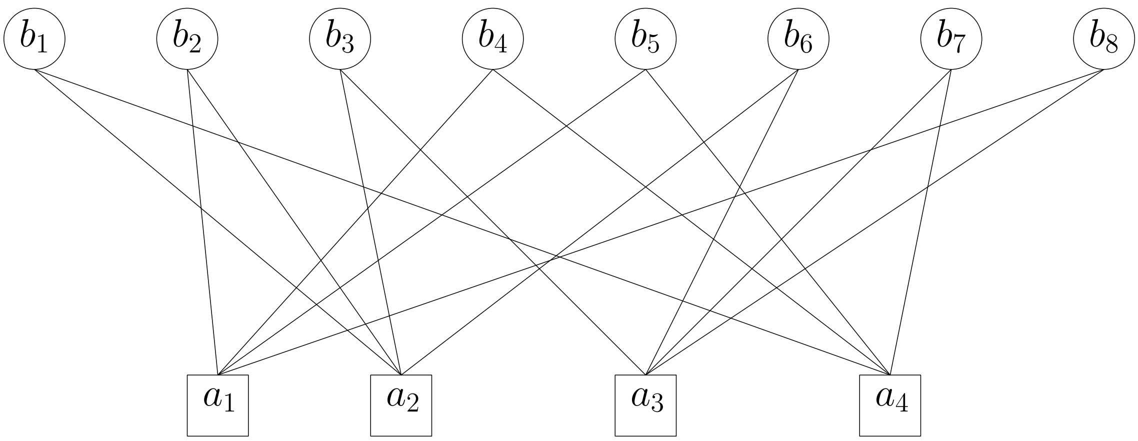

Figure 3.1.1: Tanner Graph representation of parity check matrix $\boldsymbol{\theta}$.

3.1.2 Sum product - Belief Propagation

In this subsection, the so-called Sum-product algorithm is introduced. This algorithm emerged from Bayesian inference methods, for instance, belief propagation. For the decoding operation, the marginal posterior distribution of each bit node and check node on a *tanner graph* is computed. Although, this distributions only compute the exact values if the *tanner graph* had no loops and no cycles, thus all the present elements can be uncorrelated. If the *tanner graph* had cycles, it can involve an iterative process of decoding. From the transmitted information between bit nodes and check nodes (circles and squares in 3.2.1, respectively), many iterative algorithms can be considered for the decoding process. These algorithms are based on soft decision message passing, taking on evidence the sum-product method. It is similar to hard decision *bit-flipping* algorithm, although the message passing between nodes are probabilities.

Let us start by considering the Sum-product algorithm which is based on belief propagation. For sake of simplicity it is denoted the variable $B_{j/i}$, which it symbolizes the set of B_j, except the bit of ith position and, consequently, $A_{i/j}$ illustrates the set of A_i, except the bit of jth position. In order to produce acceptable estimates, A_i must be large in spite of B_j being small, due to a large number of bits in B_j.

However, it must be taken under consideration that a large number of bits in B_j can easily provide low estimation for each bit nodes b, since it is more probable to have errors in others $B_{j' \neq j}$.

In this iterative process studied and optimized in [Joh10], it was taken in examination the passed information between bit nodes and check nodes by applying the log-likelihood ratio (LLR), characterized by *a posteriori* probability. For a binary random variable X, it is possible to represent the logarithm of probability ratio by

$$LLR(X) = log\left(\frac{P(X=0)}{P(X=1)}\right) = log\left(\frac{P(X=0)}{1-P(X=0)}\right), \tag{3.2}$$

to be noted that having zero as a result, if $P(X = 0)$ will be equal to 1/2. The likelihood probability of X is expressed by the probability of bit note b_j being one. Therefore, it can be represented by the conditional probability expression as $p = p(X|b_j = 1)$.

The first step of the decoding process is yielded by computing the extrinsic message from check node a_i to bit node b_j, which indicates the LLR probability for each j, and for each i, defined by

$$E_{j,i} = 2tanh^{-1} \prod^{i' \in B_{j/i}} tanh(M_{j,i'}/2). \tag{3.3}$$

Furthermore, the message $M_{j,i}$ represents the intrinsic information arrived at check node a_i from all connected bit nodes. On the other hand, $M_{j,i'}$ is represented similar to the previous definition, although, it excludes the message coming from target bit node b_i.

The second step is defined by a bit node update, represented in (3.4). Each bit node i has as an input the *a priori* probability LLR, thus, it is computed the sum of the input LLR with the others LLR from connect check nodes. Therefore, each bit node has *a priori* information L and all the L's from the check nodes connected to it.

$$L_i = LLR_i + \sum_{j \in A_i}^{N} E_{j,i}. \tag{3.4}$$

The update is done by completing the message from bit nodes to check nodes, accordingly

$$M_{i,j} = LLR_i + \sum_{j' \in A_i, j \neq j'}^{N} E_{j',i}, \tag{3.5}$$

Finally, the decoding process is followed by the hard decision, based on eq. (3.4), where is defined the decoded vector $\hat{x}$, by

$$\hat{x}^{SP} = \begin{cases} 0, & \text{if} \quad L_i \geq 0; \\ 1, & \text{if} \quad L_i < 0. \end{cases} \tag{3.6}$$

If the syndrome syn of the followed expression was zero, it is possible to prove that $\hat{x}$ is a valid codeword.

$$syn = \hat{x}^{SP} \boldsymbol{\theta}^T. \tag{3.7}$$

If not, the algorithm returns to the first step. In general, an algorithm implements a maximum number of iteration as a stopping criteria. The marginal posterior $p(x_j)$ can be obtained as the product of all messages that arrives to node x_j.

The iterative process of the described algorithm it is presented in Fig. 3.2.1, where it is showed the bit node and chekc node update.

3.2 Generalized Approximate Message Passing

In this section, it is considered the receiver design so as to cope with the strong nonlinear distortion effects that were introduced by HPA's and DAC's at the transmitter side. For this purpose, the receiver structure can be based on quadratic

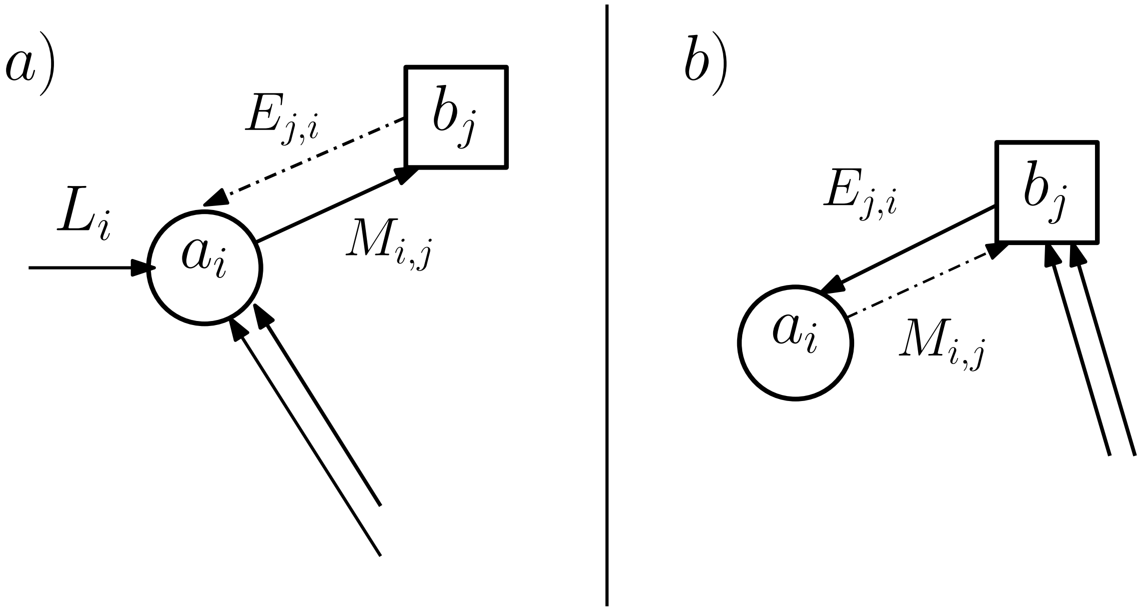

Figure 3.1.2: Message passing between nodes. In *a*) is illustrated the bit node a_i update and in *b*) is illustrated the check node b_j update on *sum product algorithm*.

Gaussian approximations and BP. The receiver presented in this section employs the so-called GAMP loopy BP [Ran10; SR15]. This algorithm arises from the state of decouple the estimation problem in an iterative algorithm based on scalar values, in order to turn it computationally efficient and less complex than other techniques that are available to estimate the input functions. Analogous with wireless communication models, it is needed to estimate the input data signal $\mathbf{x}$, based on observations of $\mathbf{y}$.

It is also possible to compute two sides of the algorithm: the first one is *Max-Sum* loopy BP which computes an approximation of *Maximum a posteriori* (MAP) estimation of $\mathbf{x}$ and $\mathbf{z}$. The second one is Sum-product loopy BP, which realizes an approximation of MMSE estimation of $\mathbf{x}$ and $\mathbf{z}$. Receivers based on the GAMP algorithm were already shown to be very effective to cope with nonlinear distortion effects in the context of OFDM [ZDy ; Zhi17b], in an effort to estimate the values of the input signal $\mathbf{x}$ to decode $\mathbf{y}$.

From the Fig. 3.2.1, the unknown input data vector $\mathbf{x}$ with *a priori* probability $p(x_i)$, passes through a transform matrix $\mathbf{B}$. This transformation can be expressed as

$$\mathbf{z}_n = \mathbf{B}\mathbf{x}_n. \tag{3.8}$$

As it can be seen in Fig. 3.2.1, the output side is viewed as observations, the received vector is passed trough a probability conditional function $p(y_i|z_i)$, and to sum up it turns on the known output vector $\mathbf{y}$.

In order to extend the GAMP algorithm to the main purpose, instead of the described equations in (2.2) and (2.11), for a given $\mathbf{B}$ matrix transformation on the system, the received signal can be defined as

$$\mathbf{y}_n = \mathbf{B}\mathbf{x}_n + \nu_n. \tag{3.9}$$

Recall here that $\mathbf{B}$ represents the unitary matrix with dimensions $N_T \times N_T$, which results from the precoding of SVD operation. This signal is submitted to the non-linear block characterized by $f(\cdot)$ in (2.18), leading to the equivalent general statement problem for the generalized approximate message passing algorithm, described by

$$\mathbf{z}_n = f(\mathrm{Re}(\mathbf{B}\mathbf{x}_n\}) + jf(\mathrm{Im}\{\mathbf{B}\mathbf{x}_n\}) + \nu_n, \tag{3.10}$$

where $\boldsymbol{\nu_n}$ is AWGN, characterized by zero mean and variance σ_ν, which is an independent and identically distributed (i.i.d.) Gaussian random variable, with a QPSK modulation for an input vector $\boldsymbol{x}$. The PDF of the corresponding channel transition is represented by

$$p_{Y|Z}(y|z) = \frac{1}{\sqrt{2\pi\sigma_n}} e^{-\frac{y-z}{2\sigma_n}}. \tag{3.11}$$

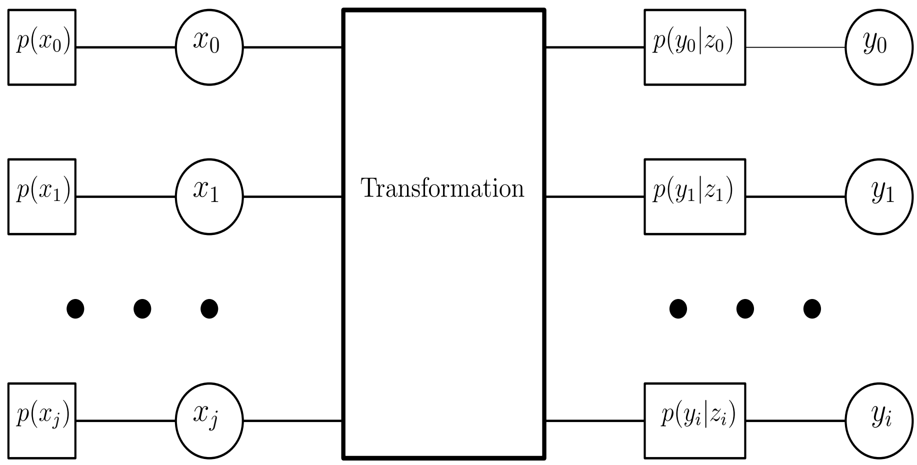

Figure 3.2.1: Factor Graph for the estimation problem. The input nodes x_j are connected to output nodes z_i by a given matrix transformation, for each input node j and output node i. The z_i variable represents the linear precoding $z = \mathbf{B}x$.

The estimation of $x(n_{it})$ and $z(n_{it})$ for the iteration n_{it} of GAMP algorithm is based on two main steps:

(a) Estimate the output nodes: it is estimated *a posteriori* $p(z_j|\mathbf{y})$, through the parameters $\hat{p}, \hat{z}$ and $\hat{s}$, and respective variances. It is also needed to select a function $g_{out}(\hat{p}, \mu_p, y)$.

(b) Estimate the input nodes: it is estimated *a posteriori* $p(x_j|\mathbf{y})$, through the parameter $\hat{r}$, and respective variances. Is is also needed to select a function $g_{in}(\hat{r}, \mu_r,)$.

Firstly, it is initialized the parameters $\tilde{x}_k(1) = 0$, $\hat{s}_k(n_{it}) = 0$ and $\mu_x(1) = 1$, although the GAMP algorithm is relatively robust to initial values.

In each iteration, the GAMP algorithm is performed for real and complex part of $\mathbf{Bx}_n$ in parallel, accordingly with (3.10).

For the first step of a given iteration n_{it}, it is estimated the parameter values of $\hat{p}$, $\hat{z}$ and $\hat{w}$, as well as their respective variances μ^p, μ^z and μ^w, for $n_{it} = 1, 2, ..., n_{itmax}$, according to the following recursions:

(1) Initialization: Set $n_{it} = 0$ and set $\hat{x}(1) = 0$, $\mu^x(1) = 0$, $\hat{w}(0) = 0$.

(2) Output linear step: for each i,

$$\mu_i^p(n_{it}) = \frac{1}{N_T} \sum_{j=0}^{N_T-1} \mu_j^x(n_{it}), \tag{3.12}$$

$$\hat{p}_i(n_{it}) = \sum_{j=0}^{N_T-1} B_{i,j}(\hat{x}_j(n_{it})) - \mu_i^p(n_{it})\hat{w}_i(n_{it} - 1), \tag{3.13}$$

$$\hat{z}_i(n_{it}) = \frac{1}{\Theta} \int_{-\infty}^{\infty} z e^{-\frac{(y_i - f(\boldsymbol{Bx}))^2}{2\sigma_v^2} - \frac{(\hat{p}_i(n_{it}) - z)^2}{2\mu_i^p(n_{it}))}} dz, \tag{3.14}$$

$$\mu_i^z(n_{it}) = \frac{1}{\Theta} \int_{-\infty}^{\infty} z^2 e^{-\frac{(y_i - f(\boldsymbol{Bx}))^2}{2\sigma_v^2} - \frac{(\hat{p}_i(n_{it}) - z)^2}{2\mu_i^p(n_{it}))}} dz - (\hat{z}_i(n_{it}))^2, \tag{3.15}$$

where the the auxiliary normalization Θ is defined by

$$\Theta = \int_{-\infty}^{\infty} e^{-\frac{(y_i - f(\boldsymbol{Bx}))^2}{2\sigma_v^2} - \frac{(\hat{p}_i(n_{it}) - z)^2}{2\mu_i^p(n_{it}))}} dz. \tag{3.16}$$

(3) Output nonlinear step: for each i,

$$\hat{w}_i(n_{it}) = g_{out}(\hat{p}_i(n_{it}), \mu_i^p(n_{it}), y_i), \tag{3.17}$$

$$\mu_i^w(n_{it}) = -\frac{\partial}{\partial \hat{p}} g_{out}(\hat{p}_i(n_{it}), \mu_i^p(n_{it}), y_i). \tag{3.18}$$

(4) Input linear step: for each j,

$$\mu_j^r(n_{it}) = \left(\frac{1}{N_T} \sum_{i=0}^{N_T-1} \mu_i^w(n_{it}) \right)^{-1}, \tag{3.19}$$

$$\hat{r}_j(n_{it}) = \tilde{x}_j(n_{it}) + \mu_j^r(n_{it}) \sum_{i=0}^{N_T-1} B_{i,j}^*(\hat{w}_i(n_{it})). \tag{3.20}$$

(5) Input nonlinear step: for each j,

$$\hat{x}_j(n_{it}+1) = g_{in}(\hat{r}_j(n_{it}), \mu_j^r(n_{it})), \tag{3.21}$$

$$\mu_j^x(n_{it}+1) = -\mu_j^r(n_{it}) \frac{\partial}{\partial \hat{r}} g_{in}(\hat{r}_j(n_{it}), \mu_j^r(n_{it})). \tag{3.22}$$

Chapter 4

Receiver Design

In this chapter, it is considered the sub-optimum receiver design for MIMO systems in the presence of nonlinear distortion effects. This design makes use of the GAMP concept, introduced in the sec. 3.2. The underlying idea behind the proposed receiver is that the transmitter can be regarded as two sets of nodes. The input nodes are associated to the mapping procedure and the output nodes are associated to the nonlinear operation before each transmit antenna. The input and output nodes are connected by the inverse DFT and precoding matrices, leading to what could be regarded as a fully, but loosely, connected Tanner graph, as shown in Fig. 4.0.1. Since the graph is loopy, conventional belief propagation techniques are not suitable to perform the decoding procedure.

The proposed receiver structure is based on quadratic Gaussian approximations and BP. It employs the extension of GAMP with sum-product loopy-BP (LBP) [Ran10; SR15] and, it is based on the GAMP algorithm presented [ZDy ; Zhi17b], where it was already shown the performance results, in SISO OFDM systems.

The receiver can be described as the sum-product GAMP, which approximates the MMSE. For a given $\mathbf{B}$ matrix transformation on the system[1], it can be defined the problem of estimating the input signal $\mathbf{x}$ to decode the known signal $\mathbf{y}$. In order to extend the GAMP algorithm, firstly it is denoted the received signal as

$$\mathbf{Y} = \mathbf{B}^H \mathbf{X} + N. \tag{4.1}$$

Concerning the second and third steps of a given iteration n_{it}, it is estimated

[1] For the sake of simplicity, it is removed the dependence with k in the following.

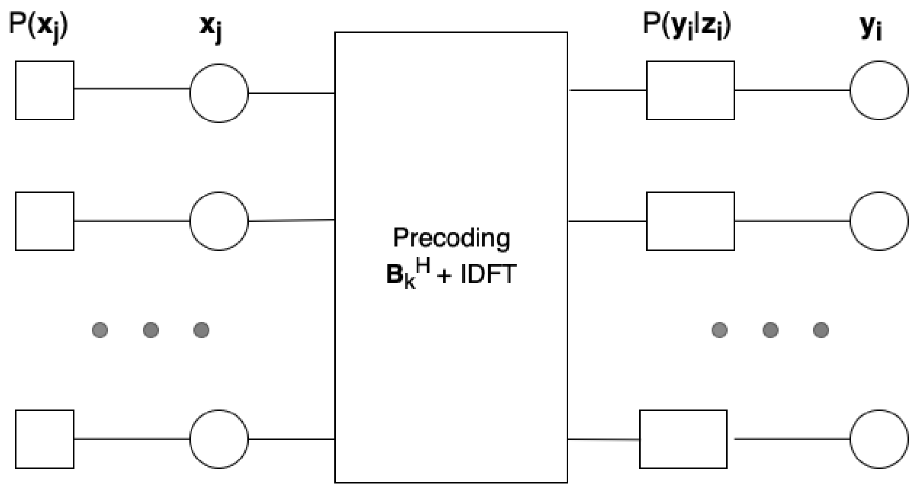

Figure 4.0.1: Factor Graph for the estimation problem. The input nodes x_j are connected to output nodes z_i by inverse DFT and precoding matrix, for each input node j and output node i. The z_i variable represents the linear proceeding $z = B_k^H x$.

the parameter values of $\hat{p}_i$, $\hat{z}_i$ and $\hat{w}_j$, as well as their respective variances μ_i^p, μ_i^z and μ_i^s. This process realizes the message passing between conditional probability nodes $p(z_i|x_i)$ to input nodes x_j, as it was described in (3.12) and (3.18).

In order to simulate the sum-product GAMP, the output function g_{out} is defined as

$$g_{out}(\hat{p}, \mu^p, y) = \frac{\hat{z}_0 - \hat{p}}{\mu^p}, \tag{4.2}$$

where,

$$\hat{z}_0 = E[z|(\hat{p}, \mu^p, y)]. \tag{4.3}$$

The expectation of (4.3) can be expressed over distribution $p(z|(\hat{p}, \mu^p, y))$. In its turn, the negative partial derivative of $g_{out}(.)$ is defined by,

$$-\frac{\partial}{\partial \hat{p}} g_{out}(\hat{p}, \mu^p, y) = \frac{1}{\mu^p}\left(1 - \frac{var[z|\hat{p}, \mu^p, y]}{\mu^p}\right). \tag{4.4}$$

On the fourth and fifth steps, it is estimated the parameter $\hat{r}$ and $\hat{x}$, with their respective variance μ^r and μ^x, accordingly to (3.19 - 3.22). This second main process realizes the message passing between x_j nodes to probability nodes which follows a posterior marginal $P(z_i|\mathbf{y})$ distribution.

In order to simulate the estimated value of $\hat{x}$, presented in (3.21), it is necessary to select a $g_{in}(.)$ and $g'_{in}(.)$, equivalently to

$$g_{in}(\hat{r}, \mu^r) = E[x|\hat{r}, \mu^r], \tag{4.5}$$

and

$$\mu^r \frac{\partial}{\partial \hat{r}} g_{in}(\hat{r}, \mu^p) = var[x|\hat{r}, \mu^r]. \tag{4.6}$$

This selection of the scalar nonlinear functions, g_{in} and g_{out}, allows to implement the algorithm as a Gaussian approximation of Sum-product Loopy BP which approximates MMSE. Otherwise, this selection can be made as an approximation of Max-sum which approximates the MAP of estimates $\hat{x}$ given y. Thus, the GAMP algorithm can be seriously flexible.

Therefore, the input non-linear steps represented in (3.21) and (3.22) were defined as

$$\hat{x}_j(n_{it}+1) = \sum_{m=1}^{\sqrt{M}} \beta_m P_{m,j}, \tag{4.7}$$

and

$$\mu_j^x(n_{it}+1) = \sum_{m=1}^{\sqrt{M}} (\beta_m - \hat{x}_j(n_{it}+1)^2) P_{m,j}, \tag{4.8}$$

where,

$$P_{m,j} = \frac{e^{-\frac{\beta_m - \hat{r}_j(n_{it})^2}{2\mu_j^r(n_{it})}}}{\sum_{l=1}^{\sqrt{M}} e^{-\frac{\beta_l - \hat{r}_j(n_{it})^2}{2\mu_j^r(n_{it})}}}. \tag{4.9}$$

The vector β_m represents the adopted constellation scheme for the real and imaginary parts and M is the total number of constellation points. For a QPSK constellations, $\beta_m = [-1 + 1]$ and $M = 4$. At each n_{it} iteration, the squared Euclidean distance between received vector $\mathbf{x}$ and the previously vector $\mathbf{x}(n_{it}-1)$ is calculated. This quantity is defined by

$$E(n_{it}) = ||\mathbf{x}(n_{it}) - \mathbf{x}(n_{it}-1))||^2 < \epsilon. \tag{4.10}$$

It is important to define a stop criteria until the convergence of algorithm is done. The stop criterium considered in the proposed receiver is triggered when the squared Euclidean distance between iterations reaches a given value ϵ.

4.1 Performance Results

4.1.1 Single Carrier MIMO-SVD

On the first scenario, it is presented a MIMO-SVD system characterized by $N_T = N_R$. The channel coefficients are assumed to be uncorrelated and to have a Rayleigh fading distribution. The objective of the system is to transmit in parallel, $C = min(N_T, N_R)$ data streams. Each signal component was chosen accordingly to a QPSK modulation scheme (i.e., in the form $s_n^{(c)} = \pm 1 \pm j$) and each data stream has 512 symbols. After the precoding operation, there is a set of ADC's with $b = 8$

bits of resolution and normalized clipping level s_M/σ_x. The choice of $b = 8$ bits of resolution assures that the nonlinear distortion effects are mainly conditioned by the normalized clipping value. A perfect channel estimation as well as a perfect time and frequency synchronization are considered.

The maximum number of iterations choice can be quiet flexible. However, when it is tested with a large number, the algorithm has slow running, with large error floors. The structure of GAMP algorithm is illustrated in Fig. 4.1.1, where it is represented the blocks of output and input nonlinear steps which produce the above described parameters, as well as the precoding and decoding operations, associated to the matrices $\mathbf{B}$ and $\mathbf{A}^H$, respectively.

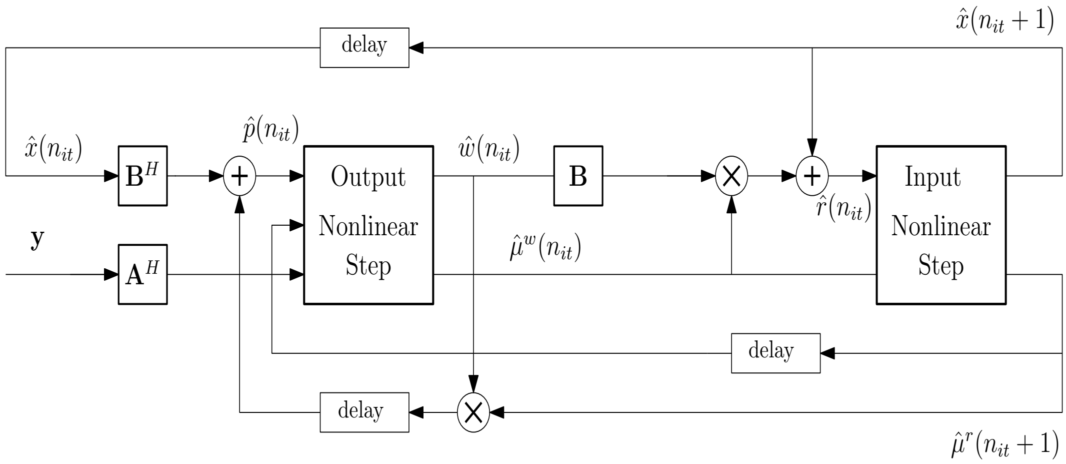

Figure 4.1.1: Block diagram of the MIMO-SVD receiver.

In Fig. 4.1.2, it is showed the BER performance of the system for different number of iterations n_{it}. A maximum value of $n_{it} = 7$ is adopted, since only marginal gains were observed for larger values.

Fig. 4.1.3 shows the BER performance for a MIMO-SVD with $N_T = N_R = 4$ configuration, and considering different values of normalized clipping level s_M/σ_x. Clearly, the BER performance of conventional receivers is very poor when low values of clipping level are considered. However, the GAMP receiver is able to improve it substantially, allowing gains well above 16 dB when BER is 10^{-3}.

In the following results, a constant value of $s_M/\sigma_x = 1.0$ is adopted. Fig. 4.1.4 considers a 4×4 MIMO scheme and Fig. 4.1.5 considers a 64×64 MIMO scheme.

Clearly, the receiver is powerful enough to cope with nonlinear distortion effects, allowing even better performance than for the linear transmission scenario. In Figs. 4.1.6 and 4.1.7, it is considered an even more severe nonlinear characteristic with normalized clipping level $s_M/\sigma_x = 0.5$. Even under these strong nonlinear distortion levels, the receiver has good performance, outperforming the linear

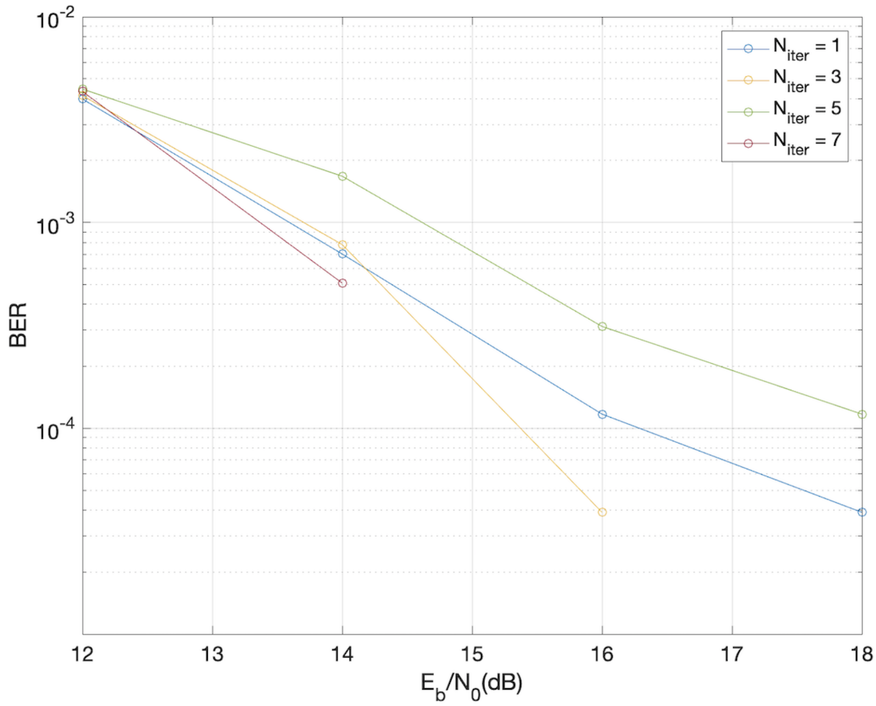

Figure 4.1.2: BER performance of the GAMP receiver with different number of iterations, for a 4×4 SVD MIMO scheme.

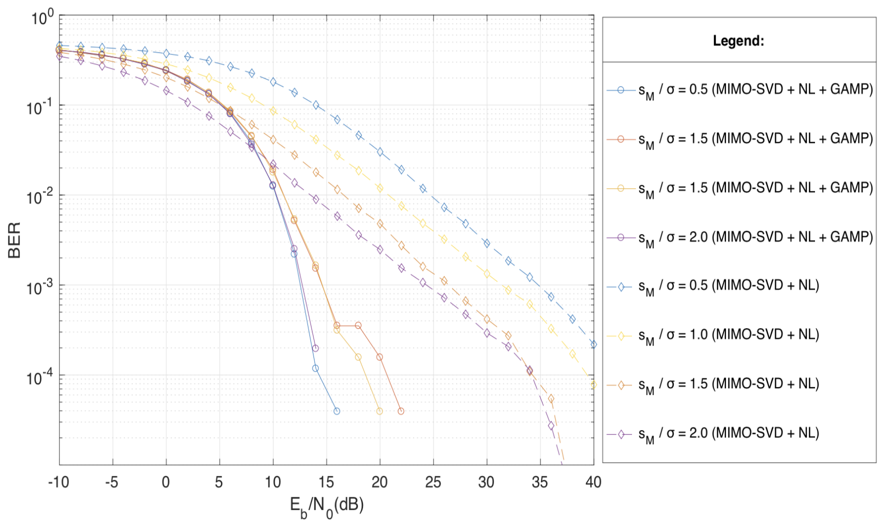

Figure 4.1.3: Average BER performance of 4×4 MIMO-SVD system for different normalized saturation levels s_M/σ_x.

scenario. In fact, not only the system has substantial gains on the required E_b/N_0 for a given BER, but also the BER values decrease sharply with E_b/N_0, which means that it is feasible to take advantage of diversity effects that are created by the nonlinear operation.

The estimation of transmitted signals is well concluded for a MIMO-SVD system, even in presence of nonlinear distortion effects.

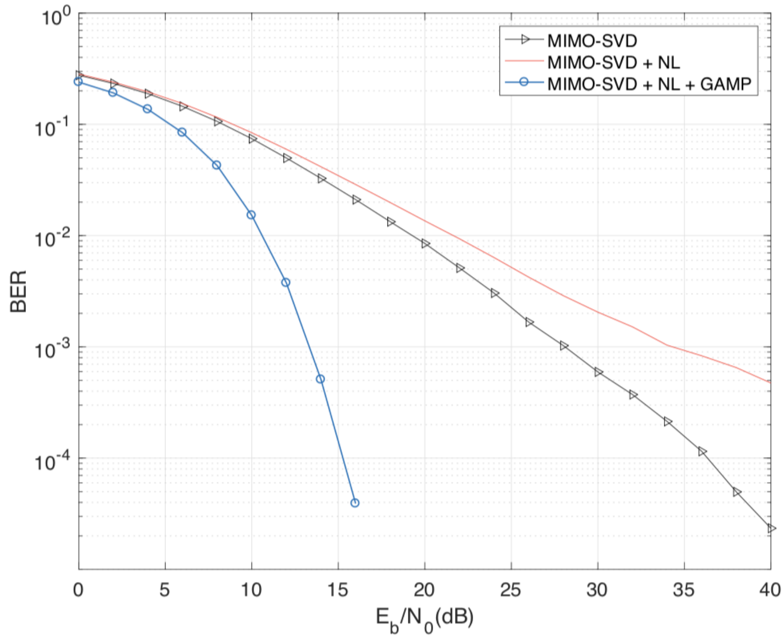

Figure 4.1.4: Average BER performance of 4×4 MIMO-SVD system considering a normalized clipping level $s_M/\sigma_x = 1.0$.

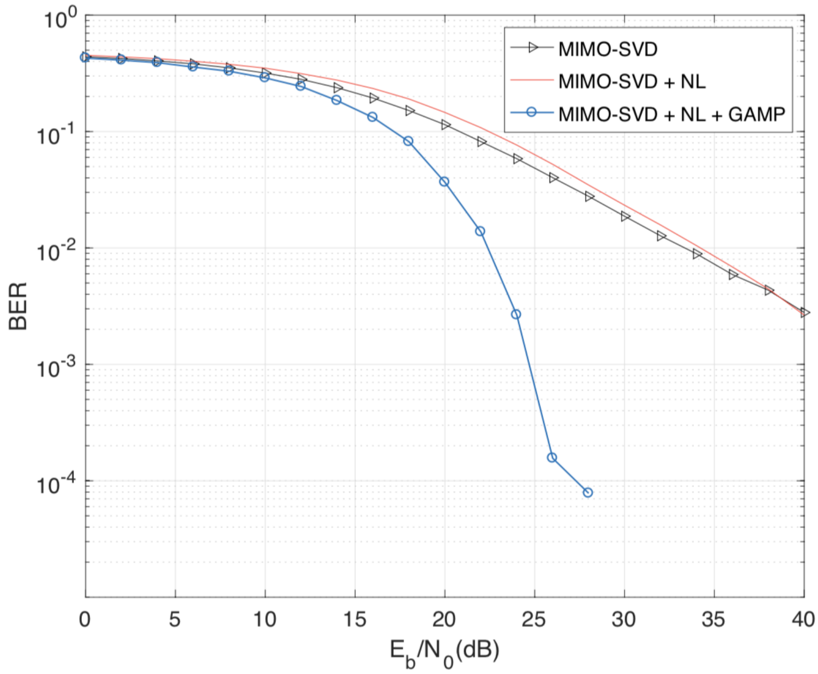

Figure 4.1.5: Average BER performance of 64×64 MIMO-SVD system considering a normalized clipping level $s_M/\sigma_x = 1.0$.

4.1.2 MIMO-OFDM

In this second section, it is presented a set of performance results for MIMO-OFDM schemes with low resolution DACs employing the proposed detection

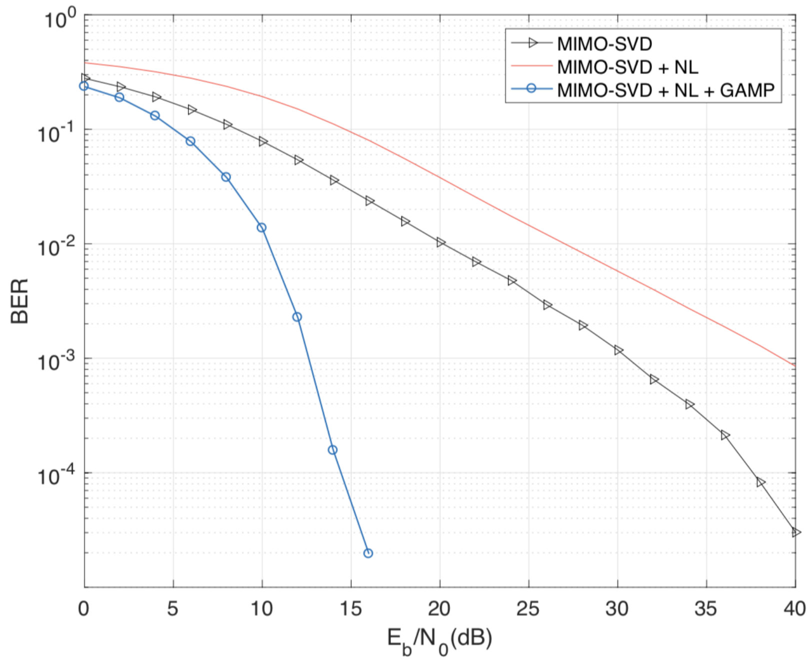

Figure 4.1.6: Average BER performance of 4×4 MIMO-SVD system considering a normalized clipping level $s_M/\sigma_x = 0.5$.

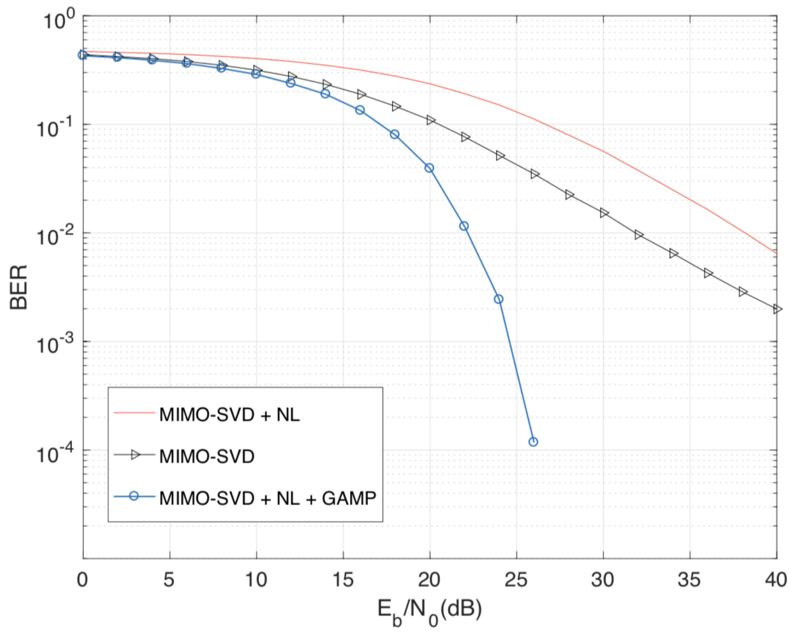

Figure 4.1.7: Average BER performance of 64×64 MIMO-SVD system considering a normalized clipping level $s_M/\sigma_x = 1.0$.

technique based on the GAMP algorithm. It is also obtained $N_T \times N_R$ MIMO SVD schemes with $N_T = 4$ transmit antennas and contrastive values of the number of receive antennas N_R. It is considered an OFDM signals with $N = 512$ subcarriers and an oversampling factor $J = 4$.

In this system, it is transmitted in parallel $C = \min(N_T, N_R)$ independent OFDM signals, each one with N subcarriers. The data symbols are the same that were presented previously, under a QPSK constellation scheme, with symbols in the form $S_k^{(c)} = \pm 1 \pm j$ selected from the data bits under a Gray mapping rule. The performance was obtained with a Monte-Carlo simulation with 1000 runs.

The structure of the receiver is depicted in Fig. 4.1.8. The received signal is passed to the frequency-domain by a set of DFT operations, followed by the detection procedure associated to the matrices $\mathbf{A}_k^H$ to complete the SVD decomposition. Next, it is showed the output and input nonlinear steps, which provide several auxiliary variables exchanged between them. Suitable DFT/IDFT and $\mathbf{B}_k$ operations are placed between these steps, which are repeated several times.

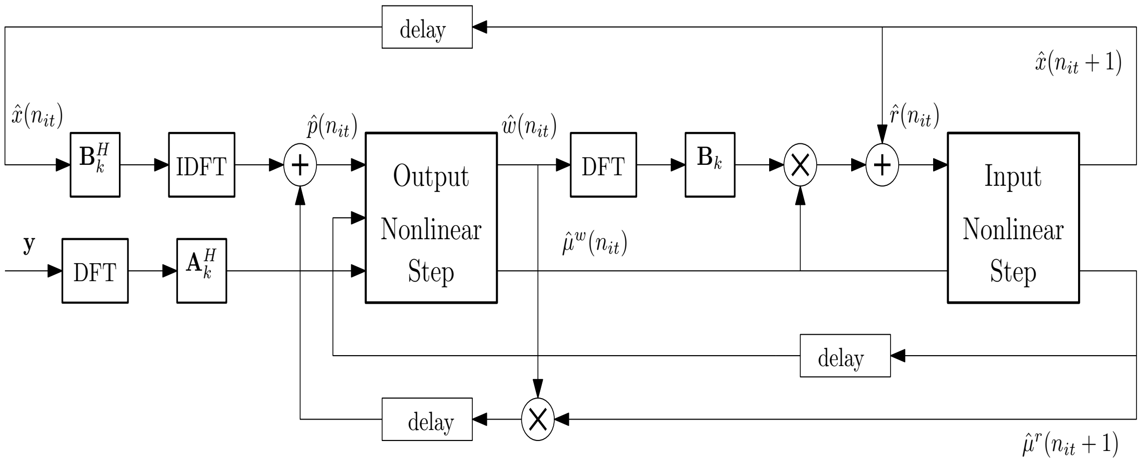

Figure 4.1.8: Block diagram of the MIMO-OFDM receiver.

Fig. 4.1.9 shows BER performance of a 4×4 MIMO-OFDM scheme for conventional receivers (considering both linear and nonlinear transmissions) and for the proposed GAMP receiver. To isolate the nonlinear degradation from the performance degradation associated to low power singular values, a scenario with unitary singular values, i.e., $\lambda_k = 1$ (but still random matrices $\mathbf{A}_k$ and $\mathbf{B}_k$). It is applied $b = 2$ bits of resolution. From the figure, it can be observed that receiver based on the GAMP has a huge performance gain when compared to conventional receivers under the same nonlinear effects at the transmitter side. More extraordinary is the fact that the receiver even outperforms the linear case (i.e., DACs with infinite resolution and without clipping effects), with a performance gain of approximately 1 dB.

On the second approach, it is taken into account a more realistic scenario through a conventional multi-path channel (i.e., the singular values were not forced to be unitary), corresponding to a frequency-selective environment.

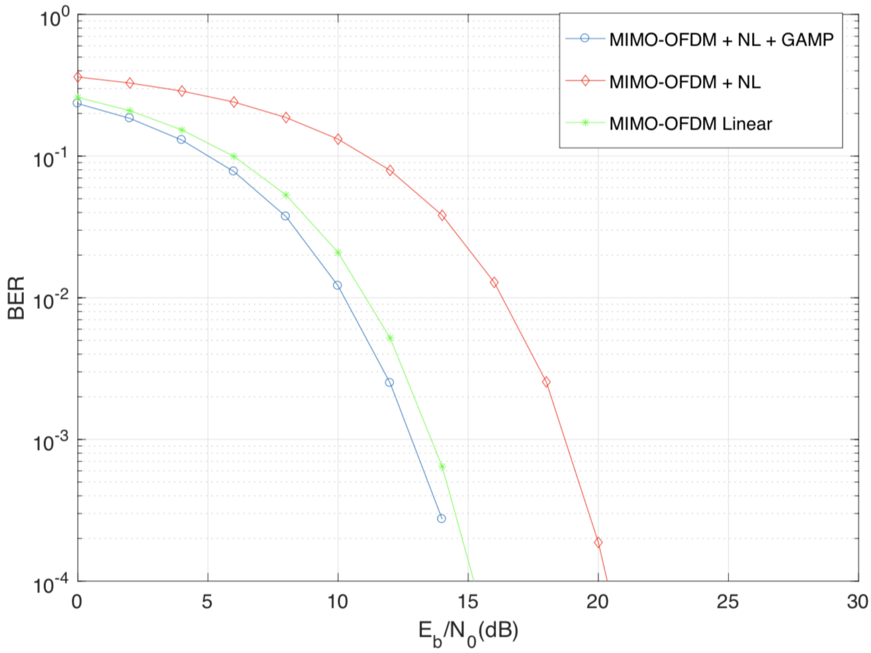

Figure 4.1.9: Average BER performance of a 4×4 MIMO-OFDM system with singular values $\lambda_k = 1$.

Fig. 4.1.10 shows the BER performance for a 4×4 MIMO-OFDM and GAMP-based receiver when the DAC's have $b = 4$ bits of resolution. For the sake of comparisons, it is also included the performance results for conventional receivers and different DAC's with different resolutions. As expected, an increase on the resolution of the DAC's leads to a better performance. However, the conventional receiver still have very large error floors, even when DAC's with $b = 6$ bits of resolution are employed. One the other hand, the proposed receiver shows a huge performance improvement when compared to the conventional receivers, without visible error floors, even outperforming linear MIMO-OFDM schemes at moderate-to-high values of E_b/N_0.

Fig. 4.1.11 shows BER performance for MIMO-OFDM systems with $N_T = 4$, DAC's with $b = 2$ bits of resolution and different numbers of receive antennas N_R. For the sake of comparisons, it is also included the performance of the corresponding linear case. As it can be noted in the figure, regardless of the value of N_R, the GAMP-based receiver outperforms the conventional receivers, even in the linear MIMO-OFDM case.

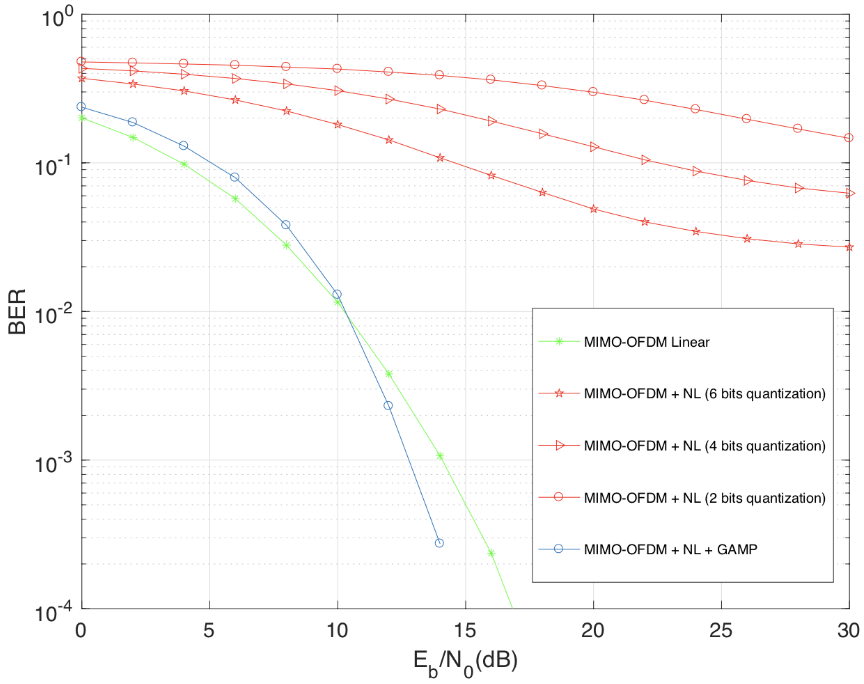

Figure 4.1.10: Average BER performance of a 4×4 MIMO-OFDM system using conventional SVD and DAC's with a different number of bits of resolution.

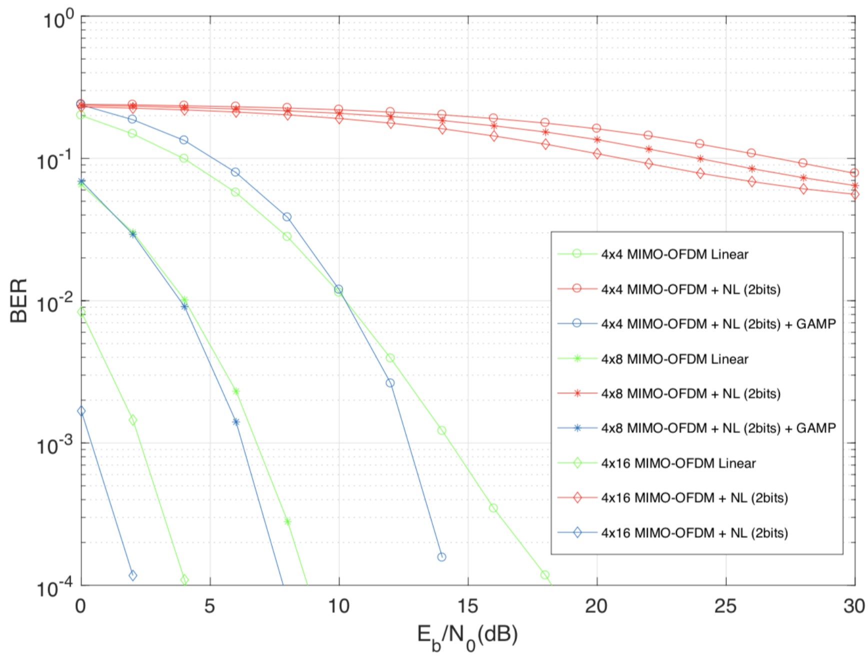

Figure 4.1.11: Average BER performance comparison of different MIMO-OFDM schemes.

4.1.3 MIMO SC-FDE

In this section, BER performance results of the proposed GAMP receiver fo MIMO SC-FDE systems are presented. It is defined N_T transmit antennas and N_R reception antennas, combining a $N_T \times N_R$ MIMO schemes with SVD technique. The considered signal has $N = 512$ as the block size and it is applied the same QPSK modulation of the previous section. It should be noted that the whole process of transmitter is on time-domain. To characterize the nonlinear distortion, we used low resolution quantizers with different resolutions. At the receiver side, it was assumed the perfect knowledge of the channel information. The performance was obtained with a Monte-Carlo simulation with 1000 runs.

On the first case, it was considered 4×4 scheme and the simulations were tested assuming unitary singular values, in order to isolate the performance degradation introduced by low power singular values. Under this conditions, Fig. 4.1.12 shows BER performance for linear, nonlinear and GAMP receivers with FDE. For both linear and nonlinear cases, the results for each transmission stream are presented. From the figure, it is possible to observe that the proposed receiver can achieve better performance than the 1st, 2nd and 3rd stream. Moreover, it is also implied that GAMP receiver outperforms the conventional average performance of MIMO-SVD schemes.

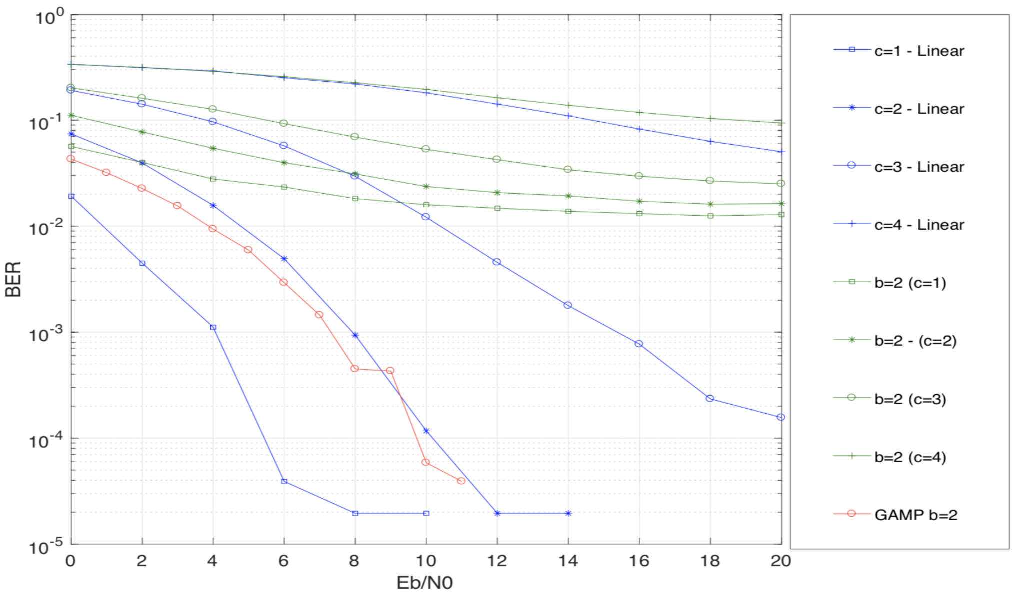

Figure 4.1.12: BER performance results of 4×4 MIMO-SVD SC-FDE, for Linear, Nonlinear ($b = 2$) and Average Nonlinear+GAMP($b = 2$) schemes, forcing unitary singular values Λ_k

On the second case, it was considered the same scheme as the previous case, however it was presented with normal singular values Λ_k and with a simple multi-path channel modeled as a frequency-selective fading, which follows a Rayleigh distribution, with 8 taps. The BER performance results are showed in Fig. 4.1.13.

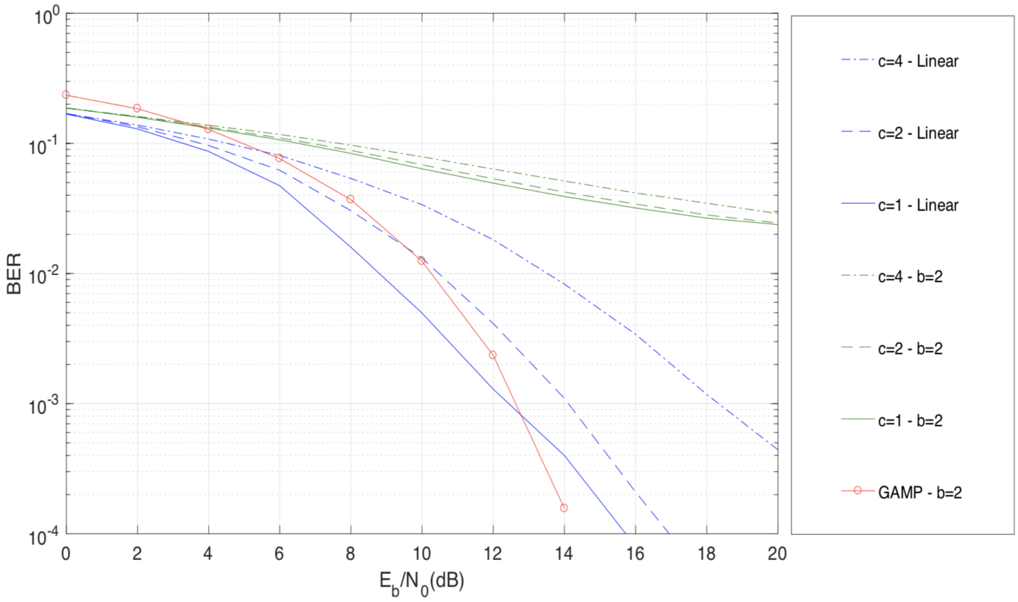

Figure 4.1.13: BER performance results of 4×4 MIMO-SVD SC-FDE Linear, Nonlinear and Nonlinear+GAMP cases, with $b = 2$, for normal singular values Λ_k.

In order to evaluate the impact of the number of bits of resolution, it is presented in Fig. 4.1.14, the average BER performance of the GAMP receiver when it was employed DAC's with $b = 1, b = 2$ and $b = 3$ bits of resolution, and the BER performance for all different streams of the nonlinear and linear structure. From the Fig. 4.1.14, it is clear that the proposed receiver shows a better performance with 3 bits resolution, although it is suitable to operate with the lower quantization resolution. For lower BER values, the GAMP receiver performance with one quantization bit will be lightly affected at higher E_b/N_0.

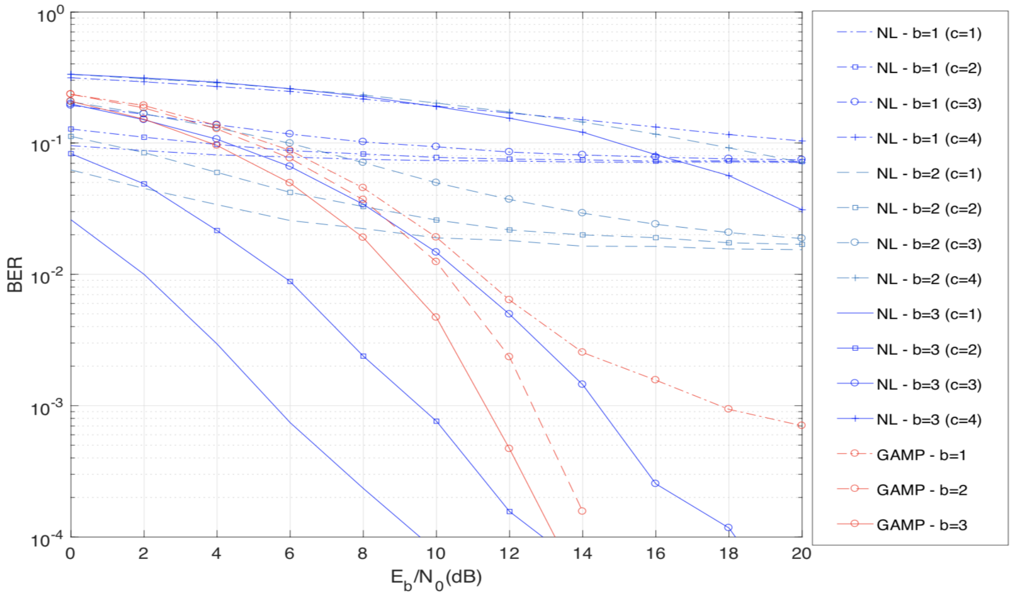

Figure 4.1.14: BER performance results of 4×4 MIMO-SVD SC-FDE Nonlinear and Nonlinear+GAMP cases, for different DAC resolution and respective clipping level.

Chapter 5

Conclusions and Final Remarks

5.1 Conclusions

In Chapter 2, it was made an introduction to MIMO transmission scheme, where it was showed the SVD decomposition of channel matrix and how a MIMO system is developed. The SVD allows the transmission of parallel data streams and it can be seen as an optimal solution. However, the SVD performance is conditioned by the performance of the worst stream. Furthermore, it was introduced the OFDM technique in order to extend to the MIMO-OFDM system. Further, models for quantization and nonlinear distortion introduced by DAC's and HPA's, respectively, were introduced. Lastly, it was introduced the MIMO SC-FDE system.

In Chapter 3, the LDPC codes were briefly described. It was also represented the parity check matrix based on a *Tanner* graphs. One of the methods of LDPC decoding is based on belief propagation between check nodes and bit nodes, described as sum product algorithm. As a consequence, it was presented an estimation decoding method that allowed nonlinear transformation and Gaussian inputs.

At last, in Chapter 4, it was exposed the performance of combination of MIMO techniques with a BP algorithm. On the first scheme MIMO-SVD, the receiver showed to be efficient on a nonlinear distortion scenario and flat-fading environment. On the second scheme, the implemented receiver constitutes a good alternative in strongly nonlinear MIMO-OFDM scenarios. Thanks to the fact that the nonlinear distortion term has some information on the transmitted signals that can be used to improve the performance. The problem with very strong nonlinearities is that the GAMP may start to have difficulty to achieve the optimal performance. Moreover, it should be pointed out that this is achieved with only a moderate increase on the receiver complexity. It increased with, essentially, a pair DFT/IDFT and the $\mathbf{B}_k$ and $\mathbf{B}_k^H$ operations for each iteration. The results showed the validity of GAMP in the presence of non-linear distortion induced by DAC. Although it is not considered the ADC of the receiver which can decrease the performance of the presented system.

According to previous results, it is clear that BER performance is worst for the lower singular values. It can be taken in consideration an interleaver and a de-interleaver operation, at both transmitter and receiver scheme, respectively. For each subcarrier, the interleaver could be placed before the precoding operation. Thereby the interleaving process can combine all different streams in equal parts. Then, at the receiver side, it could be adopted a de-interleaving after decoding operation. Therefore, the channel can be seen as frequency-selective through this operation. The performance on SC-FDE can be conditioned by one bit quantizer for moderate values of E_b/N_0, as it was showed.

To summarize, the greatest breakthrough of this dissertation was achieved by demonstrating the performance of the receiver to deal with nonlinear effects which allows it to achieve even better performance than linear systems.

5.2 Future Work

This dissertation was fulfilled with the purpose of analyze MIMO signal transmission with strong nonlinear distortion effects. With an approximation of the next generation of wireless communication, it is suitable to extend the results to a massive MIMO configuration. Moreover, other improvements on the GAMP algorithm can also be developed.

For a future research, it would be interesting to join some type of error correction codes to the previous implemented transmission and reception structures, in order to extend the performance results, for instance, LDPC codes (regular or irregular) or turbo codes. Other type of modulation can be contemplated too, such as 16-QAM. In addiction, other models of nonlinearity can be studied, since the choice of this nonlinearity can be adapted to improve the system performance.

Bibliography

[AFS10] K. A. Farhan and J. Speidel. “Advances in MIMO Techniques for Mobile Communications—A Survey.” In: *IJCNS* 3 (Jan. 2010), pp. 213–252. doi: 10.4236/ijcns.2010.33031.

[Afa+16] S. Afaqui, E. Garcia-Villegas, and E. Lopez-Aguilera. “IEEE 802.11ax: Challenges and Requirements for Future High Efficiency WiFi.” In: *IEEE Wireless Communications* PP (Dec. 2016). doi: 10.1109/MWC.2016.1600089WC.

[ÁT16] F. Ávila and M. Tcheou. “Bayesian Inference, Stochastic Simulation and Their Applications in Wireless Communication Systems.” In: *Journal of Communication and Information Systems* 31.1 (2016). doi: 10.14209/jcis.2016.27. url: https://jcis.sbrt.org.br/jcis/article/view/394.

[Bus52] J. J. Bussgang. “Crosscorrelation functions of amplitude-distorted Gaussian signals.” In: *Tech. Rep. 216, Research Lab. Electron* (1952).

[Don+09] D. L. Donoho, A. Maleki, and A. Montanari. “Message Passing Algorithms for Compressed Sensing.” In: *CoRR* abs/0907.3574 (2009). arXiv: 0907.3574. url: http://arxiv.org/abs/0907.3574.

[Gal63] R. G. Gallager. *Low-Density Parity-Check Codes*. 1963.

[Gue+15] J. Guerreiro, R. Dinis, and P. Carvalho. “On the Optimum Multicarrier Performance With Memoryless Nonlinearities.” In: *IEEE Transactions on Communications* 63 (Jan. 2015), pp. 498–509. doi: 10.1109/TVT.2014.2381874.

[Gue+16a] J. Guerreiro, R. Dinis, and P. Carvalho. “Massive MIMO with Nonlinear Amplification: Signal Characterization and Performance Evaluation.” In: Dec. 2016, pp. 1–6. doi: 10.1109/GLOCOM.2016.7841975.

[Gue+16b] J. Guerreiro, R. Dinis, and P. Carvalho. “On the Assessment of Nonlinear Distortion Effects in MIMO-OFDM Systems.” In: May 2016, pp. 1–5. doi: 10.1109/VTCSpring.2016.7504376.

[Gue+17] J. Guerreiro, R. Dinis, and P. Carvalho. "On the Impact of Strong Nonlinear Effects on Massive MIMO SVD Systems with Imperfect Channel Estimates." In: Sept. 2017, pp. 1–5. DOI: 10.1109/VTCFall.2017.8288010.

[Gus+05] A Gusmao, R. Dinis, and P. Torres. "Low-PMEPR OFDM transmission with an iterative receiver technique for cancellation of nonlinear distortion." In: vol. 4. Oct. 2005, pp. 2367 –2371. ISBN: 0-7803-9152-7. DOI: 10.1109/VETECF.2005.1558972.

[Hel+11] T. Helaly, R. Dansereau, and M. El-Tanany. "BER performance of OFDM signals in presence of nonlinear distortion due to SSPA." In: *Wireless Personal Communications* 64 (Jan. 2011), pp. 749–760. DOI: 10.1007/s11277-010-0217-z.

[Joh10] S. Johnson. "Introducing Low-Density Parity-Check Codes." In: (May 2010).

[LaS+08] N. LaSorte, W. J. Barnes, and H. H. Refai. "The History of Orthogonal Frequency Division Multiplexing." In: *IEEE GLOBECOM 2008 - 2008 IEEE Global Telecommunications Conference*. 2008, pp. 1–5. DOI: 10.1109/GLOCOM.2008.ECP.690.

[Liu+09] W. Liu, L. Yang, and L Hanzo. "SVD-Assisted Multiuser Transmitter and Multiuser Detector Design for MIMO Systems." In: *Vehicular Technology, IEEE Transactions on* 58 (Mar. 2009), pp. 1016 –1021. DOI: 10.1109/TVT.2008.927728.

[Mad+19] J. Madeira, J. Guerreiro, and R. Dinis. "Iterative Frequency-Domain Detection for MIMO Systems with Strong Nonlinear Distortion Effects." English. In: *10th International Congress on Ultra Modern Telecommunications and Control Systems and Workshops, ICUMT 2018*. International Conference on Ultra Modern Telecommunications and Control Systems amp; Workshops. UTD/EEA/50008/2013. Sem PDF conforme despacho. IEEE Computer Society, Jan. 2019. DOI: 10.1109/ICUMT.2018.8631239.

[Min85] J. Minkoff. "The Role of AM-to-PM Conversion in Memoryless Nonlinear Systems." In: *IEEE Transactions on Communications* 33.2 (1985), pp. 139–144. ISSN: 0090-6778. DOI: 10.1109/TCOM.1985.1096262.

[PP02] A. Papoulis and U. Pillai. "Probability, Random Variables, and Stochastic Processes, Fourth Edition." In: (Jan. 2002).

[RM13] Y. Rahmatallah and S. Mohan. "Peak-To-Average Power Ratio Reduction in OFDM Systems: A Survey And Taxonomy." In: *Communications Surveys Tutorials, IEEE* 15 (Jan. 2013), pp. 1567–1592. DOI: 10.1109/SURV.2013.021313.00164.

[Ran10] S. Rangan. "Generalized Approximate Message Passing for Estimation with Random Linear Mixing." In: *CoRR* abs/1010.5141 (2010). arXiv: 1010.5141. URL: http://arxiv.org/abs/1010.5141.

[Rap91] C. Rapp. "Effects of HPA-nonlinearity on 4-DPSK/OFDM-signal for a digital sound broadcasting system." In: Oct. 1991, pp. 179–184.

[Rap+13] T. S. Rappaport, S. Sun, R. Mayzus, H. Zhao, Y. Azar, K. Wang, G. N. Wong, J. K. Schulz, M. Samimi, and F. Gutierrez. "Millimeter Wave Mobile Communications for 5G Cellular: It Will Work!" In: *IEEE Access* 1 (2013), pp. 335–349. DOI: 10.1109/ACCESS.2013.2260813.

[Rib+15] F. C. Ribeiro, R. Dinis, F. Cercas, and A. Silva. "Receiver design for the uplink of base station cooperation systems employing SC-FDE modulations." In: *EURASIP Journal on Wireless Communications and Networking* 2015.1 (2015), p. 7. DOI: 10.1186/s13638-014-0237-6. URL: https://doi.org/10.1186/s13638-014-0237-6.

[Row82] H. E. Rowe. "Memoryless nonlinearities with Gaussian inputs: Elementary results." In: *The Bell System Technical Journal* 61.7 (1982), pp. 1519–1525. ISSN: 0005-8580. DOI: 10.1002/j.1538-7305.1982.tb04356.x.

[Rud14] A. Rudziński. "Normalized Gaussian approach to statistical modeling of OFDM signals." In: *Journal of Telecommunications and Information Technology* (Mar. 2014), p. 54.

[Sal81] A. A. M. Saleh. "Frequency-Independent and Frequency-Dependent Nonlinear Models of TWT Amplifiers." In: *IEEE Transactions on Communications* 29.11 (1981), pp. 1715–1720. ISSN: 0090-6778. DOI: 10.1109/TCOM.1981.1094911.

[Sam+02] H. Sampath, S. Talwar, J. Tellado, V. Erceg, and P. AJ. "A fourth-generation MIMO-OFDM broadband wireless system: Design, performance, and field trial results." In: *Communications Magazine, IEEE* 40 (Oct. 2002), pp. 143 –149. DOI: 10.1109/MCOM.2002.1031841.

[San+98] M. Sandell, J. Beek, and P. Börjesson. "Timing and Frequency Synchronization in OFDM Systems Using the Cyclic Prefix." In: (June 1998).

[SR15] P. Schniter and S. Rangan. "Compressive Phase Retrieval via Generalized Approximate Message Passing." In: *IEEE Transactions on Signal Processing* 63.4 (2015), pp. 1043–1055. ISSN: 1053-587X. DOI: 10.1109/TSP.2014.2386294.

[Sha48] C. E. Shannon. "A Mathematical Theory of Communication." In: *The Bell System Technical Journal* 27.3 (July 1948), pp. 379–423. DOI: 10.1002/j.1538-7305.1948.tb01338.x. URL: https://ieeexplore.ieee.org/document/6773024/.

[Sho04] A. Shokrollahi. "LDPC Codes: An Introduction." In: *Coding, Cryptography and Combinatorics*. Ed. by K. Feng, H. Niederreiter, and C. Xing. Basel: Birkhäuser Basel, 2004, pp. 85–110. ISBN: 978-3-0348-7865-4.

[Wan+00] X. Wang, R. Chen, and J. Liu. "Monte Carlo Bayesian Signal Processing for Wireless Communications." In: *Journal of VLSI signal processing systems for signal, image and video technology* 30 (Nov. 2000). DOI: 10.1007/0-306-47322-4_7.

[Wan+10] Y. Wang, K. Cunningham, P. Nagvajara, and J. Johnson. "Singular Value Decomposition Hardware for MIMO: State of the Art and Custom Design." In: *2010 International Conference on Reconfigurable Computing and FPGAs*. 2010, pp. 400–405. DOI: 10.1109/ReConFig.2010.62.

[ZDy] S. V. Zhidkov and R. Dinis. "Belief Propagation Receivers for Near-Optimal Detection of Nonlinearly Distorted OFDM Signals." In: IEEE-VTC'2019, Spring. Kuala Lumpur, May 2019.

[Zhi17a] S. V. Zhidkov. "Approaching Channel Capacity without Error Correction Coding through Nonlinear Transformation of OFDM Signals." In: *CoRR* abs/1703.03141 (2017). arXiv: 1703.03141. URL: http://arxiv.org/abs/1703.03141.

[Zhi17b] S. V. Zhidkov. "Detection of Nonlinearly Distorted OFDM Signals via Generalized Approximate Message Passing." In: *CoRR* abs/1703.01562 (2017). arXiv: 1703.01562. URL: http://arxiv.org/abs/1703.01562.